PNAS
www.pnas.org

Supplementary Information for

Transcriptomic atlas of mushroom development reveals conserved genes behind complex multicellularity in fungi

Krisztina Krizsán, Éva Almási, Zsolt Merényi, Neha Sahu, Máté Virágh, Tamás Kószó, Stephen Mondo, Brigitta Kiss, Balázs Bálint, Ursula Kües, Kerrie Barry, Judit Cseklye, Botond Hegedüs, Bernard Henrissat, Jenifer Johnson, Anna Lipzen, Robin A. Ohm, István Nagy, Jasmyn Pangilinan, Juying Yan, Yi Xiong, Igor V. Grigoriev, David S. Hibbett, László G. Nagy

László G. Nagy
Email: lnagy@fungenomelab.com

This PDF file includes:

Supplementary text
Figs. S1 to S29
Tables S1 to S2
Captions for Dataset S1 to S12
References for SI reference citations

Other supplementary materials for this manuscript include the following:

Datasets S1 to S12

Supporting Information Text

SI Materials and Methods

Strains, fruiting protocols and nucleic acid extraction. For fruiting *Coprinopsis cinerea* strain #326 (*A43mut B43mut pab 1-1*) an agar disk (5 mm in diameter) was placed on the center of YMG/T agar media (4 g yeast extract, 10 g malt extract, 4 g glucose, 10 g agar media with 100 mg tryptophane added after cooling(1)) at 37 °C for five days in the dark. When the colonies reached the 1-2 mm distance from the edge of Petri dishes they were placed into 25 °C for one week in a 12 hrs light/12 hrs dark cycle for fruiting. Fruiting body stages were defined following standard conventions(2). Exact alignment of developmental stages across species was impossible, but we made an attempt to define functionally putatively homogeneous stages to follow the general notation of mushroom developmental stages as closely as possible in each species. Nevertheless, the array of sample types differed from species to species, due to the morphological diversity of fruiting bodies or limitations in dissectability. In *Coprinopsis*, vegetative mycelium, hyphal knot, stage 1 and stage 2 primordia, young fruiting body cap, gills and stipe, fruiting body cap and stipe were harvested for RNA extraction. The hyphal knot stage was defined as an up to 0.5 mm diameter condensed hyphal aggregate. Stage 1 primordia were defined as up to 2 mm tall shaft like structures, while stage 2 primordia up to 4 mm tall fruiting body initials with visible differentiation of cap and stipe initials. Young fruiting bodies were up to 15 mm tall with a slightly elongated stipe and immature basidia. Fruiting bodies had fully extended stipes and caps, being in an early autolytic phase.

Before fruiting, *Schizophyllum commune* the H4-8a and H4-8b monokaryons(3) were grown on MM medium according to Dons et. al.(4). After dikaryon formation an agar plug (5 mm) was placed on the center of fresh MM medium at 30 °C for five days in the dark, then it was placed at 25 °C for 10 days in a 12/12 hrs light/dark cycle (cool white F18w/840), upside down. Dikaryotic vegetative mycelium, stage 1 and 2 primordia, young fruiting body and fruiting body stages were harvested for RNA-seq. We defined stage 1 primordia as up to 2 mm fruiting body initials, stage 2 primordia as 3-4 mm tall initials with an apical pit on the top, the young fruiting body as a 5-7 mm tall cup-like structure with visible pseudolamellae inside, while fully expanded ones were considered fruiting body.

Vegetative mycelia of *Lentinus tigrinus* RLP-9953-sp were maintained on MEA (20 g malt extract, 0.5 g yeast extract, 15 g agar for 1L). For fruiting a mycelial plug was placed (5 mm diameter) on modified sawdust-rice bran medium(5) (1 part wheat bran and 2 parts aspen sawdust wetted to 65% moisture for 100 ml in a 250 ml beaker). The culture was incubated for 21 days at 30 °C in the dark, then placed in a moist growth chamber at 25 °C in a 12/12 hour light/dark cycle. Vegetative mycelia, stage 1 primordia, stage 2 primordia cap and stipe, young fruiting body cap and stipe and fruiting body cap and stipe tissues were harvested for RNA-Seq. Stage 1 primordium was defined as a 5-20 mm tall white stalk-structure without any differentiation of a cap initial, stage 2 primordium was defined as a 15 – 25 mm tall stalk-like structure with a brown apical pigmentation (cap initial), young fruiting body had and up to 5 mm wide brown cap initial with just barely visible gills on the bottom, growing on a 30-40 mm tall stipe, fruiting body was 50-70 mm tall, with fully flattened (but not funnel-shaped) cap.

Phanerochaete chrysosporium RP-78 was fruited on YMPG media (10 g glucose, 10 g malt extract, 2 g peptone, 2 g yeast extract, 1 g asparagine, 2 g KH_2PO_4, 1 g $MgSO_4$ x 7 H_2O, 20 g agar for 1L with 1 mg thiamine added after cooling) covered with cellophane for 7 days at 37 °C in the dark, then placed in a moist growth chamber at 25 °C in an area with dimmed ambient light conditions, following the recommendations of Jill Gaskell (US Forest Products Laboratory, Washington, D. C., USA). Vegetative mycelium, young fruiting body and fruiting body stages were harvested for RNA extraction. Young fruiting body stage was defined as fruiting body initials that forms a compact mat

well-delimited from the surrounding vegetative mycelium, while the fruiting bodies were harvested just after they started releasing spores (visible on the lids of Petri dishes).

Rickenella mellea SZMC22713 was cultured on Fries Agar(6) for harvesting vegetative mycelium for RNA and DNA extraction. DNA for genome sequencing was extracted using the Blood & Cell Culture DNA Maxi Kit (Qiagen) from 300 mg finely ground mycelium powder according to the manufacturer's instructions. The internal transcribed spacer region was PCR amplified and sequenced to verify strain identity. For RNA-Seq, fruiting bodies were collected in November 2016 from Kistelek, Hungary (approx. coordinates: 46.546309, 19.954507). Stage 1 primordium was defined as an approximately 1 mm tall, shaft-like, pear-shaped structure, without any visible cap initial, stage 2 primordium was described as a 2-3 mm tall structure with a small cap initial, young fruiting body was defined by the 5-15 mm tall structure with a 1-2 mm wide cap, and the fruiting body was characterized by a fully expanded cap on the top of a 20-32 mm tall stipe, from the same colony.

Data for *Armillaria ostoyae* C18/19 were taken from our previous study(7), with the following stages defined: vegetative mycelium, stage 1 primordium, stage 2 primordium cap and stipe, young fruiting body cap and stipe, and fruiting body cap, stipe and gills.

For RNA extraction all samples were immediately placed on liquid nitrogen after harvesting and stored at -80 °C until use. Frozen tissues were weighed and 10-20 mg of *C. cinerea, S. commune, P. chrysosporium* and *R. mellea* and 50-75 mg of *L. tigrinus* were transferred to a pre-chilled mortar and ground to a fine powder using liquid nitrogen. We extracted RNA of *C. cinerea, S. commune, P. chrysosporium* and *R. mellea* using the Quick-RNA^{TM} Miniprep (Zymo Research), or the RNeasy Midi Kit (QIAGEN) for *L. tigrinus.* Both of the kits were used according to the manufacturer's instructions.

De novo draft genome for *Rickenella mellea.* The genome and transcriptome of *Rickenella mellea* were sequenced using Illumina platform. The genomes were sequenced as pairs of Illumina standard and Nextera long mate-pair (LMP) libraries. For the Illumina Regular Fragment library, 100 ng of DNA was sheared to 300 bp using the Covaris LE220 and size selected using SPRI beads (Beckman Coulter). The fragments were treated with end-repair, A-tailing, and ligation of Illumina compatible adapters (IDT, Inc) using the KAPA-Illumina library creation kit (KAPA biosystems).

For the Illumina Regular Long-mate Pair library (LMP), 5 ug of DNA was sheared using the Covaris g-TUBE(TM) and gel size selected for 4 kb. The sheared DNA was treated with end repair and ligated with biotinylated adapters containing *loxP*. The adapter ligated DNA fragments were circularized via recombination by a Cre excision reaction (NEB). The circularized DNA templates were then randomly sheared using the Covaris LE220 (Covaris). The sheared fragments were treated with end repair and A-tailing using the KAPA-Illumina library creation kit (KAPA biosystems) followed by immobilization of mate pair fragments on streptavidin beads (Invitrogen). Illumina compatible adapters (IDT, Inc) were ligated to the mate pair fragments and 8 cycles of PCR was used to enrich for the final library (KAPA Biosystems).

Stranded cDNA libraries were generated using the Illumina Truseq Stranded RNA LT kit. mRNA was purified from 1 µg of total RNA using magnetic beads containing poly-T oligos. mRNA was fragmented and reversed transcribed using random hexamers and SSII (Invitrogen) followed by second strand synthesis. The fragmented cDNA was treated with end-pair, A-tailing, adapter ligation, and 8 cycles of PCR.

The prepared libraries were quantified using KAPA Biosystem's next-generation sequencing library qPCR kit and run on a Roche LightCycler 480 real-time PCR instrument. The quantified libraries were then multiplexed with other libraries, and the pool of libraries was then prepared for sequencing on the Illumina HiSeq sequencing platform utilizing a TruSeq paired-end cluster kit, v4,

and Illumina's cBot instrument to generate a clustered flow cell for sequencing. Sequencing of the flow cell was performed on the Illumina HiSeq2500 sequencer using HiSeq TruSeq SBS sequencing kits, v4, following a 2x150 indexed run recipe (2x100bp for LMP).

Genomic reads from both libraries were QC filtered for artifact/process contamination and assembled together with AllPathsLG v. R49403(8). Illumina reads of stranded RNA-seq data were used as input for de novo assembly of RNA contigs, assembled into consensus sequences using Rnnotator (v. 3.4)(9). Both genomes were annotated using the JGI Annotation Pipeline and made available via the JGI fungal portal MycoCosm(10). Genome assemblies and annotation were also deposited at DDBJ/EMBL/GenBank under the accession QMKR00000000.

RNA-Seq. Whole transcriptome sequencing was performed using the TrueSeq RNA Library Preparation Kit v2 (Illumina) according to the manufacturer's instructions. Briefly, RNA quality and quantity measurements were performed using RNA ScreenTape and Reagents on TapeStation (all from Agilent) and Qubit (ThermoFisher); only high quality (RIN >8.0) total RNA samples were processed. Next, RNA was DNaseI (ThermoFisher) treated and the mRNA was purified and fragmented. First strand cDNA synthesis was performed using SuperScript II (ThermoFisher) followed by second strand cDNA synthesis, end repair, 3'-end adenylation, adapter ligation and PCR amplification. All of the purification steps were performed using AmPureXP Beads (Backman Coulter). Final libraries were quality checked using D1000 ScreenTape and Reagents on TapeStation (all from Agilent). Concentration of each library was determined using either the QPCR Quantification Kit for Illumina (Agilent) or the KAPA Library Quantification Kit for Illumina (KAPA Biosystems). Sequencing was performed on Illumina instruments using the HiSeq SBS Kit v4 250 cycles kit (Illumina) or the NextSeq 500/550 High Output Kit v2 300 cycles (Illumina) generating >20 million clusters for each sample.

Bioinformatic analyses of RNA-Seq data. RNA-Seq analyses were carried out as reported earlier(7). Paired-end Illumina (HiSeq, NextSeq) reads were quality trimmed using the CLC Genomics Workbench tool version 9.5.2 (CLC Bio/Qiagen) removing ambiguous nucleotides as well as any low quality read end parts. Quality cutoff value (error probability) was set to 0.05, corresponding to a Phred score of 13. Trimmed reads containing at least 40 bases were mapped using the RNA-Seq Analysis 2.1 package in CLC requiring at least 80% sequence identity over at least 80% of the read lengths; strand specificity was omitted. List of reference sequences is provided as Supplementary Table 1. Reads with less than 30 equally scoring mapping positions were mapped to all possible locations while reads with more than 30 potential mapping positions were considered as uninformative repeat reads and were removed from the analysis.

"Total gene read" RNA-Seq count data was imported from CLC into R version 3.0.2. Genes were filtered based on their expression levels keeping only those features that were detected by at least five mapped reads in at least 25% of the samples included in the study. Subsequently, "calcNormFactors" from "edgeR" version 3.4.2(11) was used to perform data scaling based on the "trimmed mean of M-values" (TMM) method(12). Log transformation was carried out by the "voom" function of the "limma" package version 3.18.13(13). Linear modeling, empirical Bayes moderation as well as the calculation of differentially expressed genes were carried out using "limma". Genes showing at least four-fold gene expression change with an FDR value below 0.05 were considered as significant. Multi-dimensional scaling ("plotMDS" function in edgeR) was applied to visually summarize gene expression profiles revealing similarities between samples. In addition, unsupervised cluster analysis with Euclidean distance calculation and complete-linkage clustering was carried out on the normalized data using "heatmap.2" function from R package "gplots".

Identification of developmentally regulated genes. We considered genes with a Fragments Per Kilobase Million (FPKM) value >1 to have a non-zero expression. Because differentially expressed genes can only be defined in pairwise comparisons of samples and thus didn't suit our developmental series data, we opted to use the concept of developmentally regulated gene. These were defined as any gene showing an over four-fold change in expression between any two developmental stages or tissue types and a maximum expression level of FPKM > 4 in at least one developmental stage. Comparisons between tissue types were only performed within the respective developmental stage. We distinguished developmentally regulated genes that showed over four-fold upregulation at fruiting body initiation ('FB-init' genes) and those that show over four-fold expression dynamics (up- or downregulation) across the range of fruiting body stages ('FB development genes', i.e. vegetative mycelium excluded). Note that this strategy excludes genes showing highest expression in vegetative mycelium and no dynamics later on, to remove genes with a significant downregulation at the onset of fruiting body development (e.g. those involved in nutrient acquisition by the mycelium).

Comparative genomic approaches. To obtain characteristic InterPro domain signatures of Agaricomycetes, we assembled a dataset comprising genomes of 201 species; ranging from unicellular yeasts to filamentous and complex multicellular fungi. InterProScan version 5.24-63.0 was used to perform IPR searches. The 201 species were categorized into two major groups; mushroom-forming fungi (113 species) and all other fungi (88 species, 1 Cryptomycota, 2 Microsporidia, 2 Neocallimastigomycota, 3 Chytridiomycota, 2 Blastocladiomycota, 14 Zygomycota, 1 Glomeromycota, 38 Ascomycota, 20 non-fruiting body forming Basidiomycota). The enrichment of IPR domains was tested using Fisher's exact test and corrected for multiple testing by the Benjamini-Hochberg method in R (R core team 2016). $P<0.01$ was considered significant. Significantly overrepresented IPR domains were characterized by Gene Ontology Terms using IPR2GO.

An all-versus-all protein BLAST was performed for the six species (*A. ostoyae, C. cinerea, S. commune, L. tigrinus, P. chrysosporium, R. mellea*) and for the 201-species dataset using mpiBLAST (v.1.6.0, e-value < 1e-5, alignment length/query length > 0.5, alignment length/hit length > 0.5) with default parameters. Clustering was done using Markov Cluster with an inflation parameter of 2.0(14).

Reconstruction of alternative splicing patterns. We reconstructed patterns of alternative splicing using the RNA-Seq data for all six species. To this end, we used region-restricted probabilistic modelling (RRPM)(15) to discover alternative transcripts, as described by Gehrmann et al.. Briefly, the genome was split at gene boundaries into fragments, then all RNA-Seq reads were aligned to these fragments with STAR v2.5.3a(16), in two rounds. The first round of read alignment was run to produce a novel splice junction database, which was used to improve mapping in the second round. Using the BAM file from this alignment, Cufflinks v2.2.1(17) was run in RABT mode to predict novel transcripts. To restore the context, these sets of transcripts were projected back onto the original annotation. The resulting annotation file was filtered to remove predicted transcripts with no detectable expression (FPKM = 0) or did not have reads supporting its splice junctions. We performed read alignment using STAR again with the same two round method and the new, corrected annotation file and used the Cufflinks suite to estimate the expression level for each transcript. We then aligned reads of each RNA-Seq replicate separately to the genome with updated gene annotation. This resulted in an expression profile for each alternatively spliced transcript, in every developmental stage. We subsequently identified developmentally regulated transcripts using the same functions as described above for genes. For splicing event discovery, we used the ASpli(18) R package where we used the most significant transcript (the most abundant transcript through the developmental stages) as

the reference for event discovery. Custom scripts were used to extract stage and tissue-type specificity and distribution of spliced genes and splicing events.

Phylostratigraphic analysis. To examine the evolutionary origin of developmentally regulated genes in each species, a phylostatigraphic analysis was performed (19). First, we assembled a database containing genomes covering the evolutionary route from the most recent common ancestor of cellular organisms to the respective species, by complementing the database of Drost et al.(20). Fungal, microsporidia and plant genomes were removed from this database and substituted by 416 fungal genomes (all published), including 382 belonging to the Dikarya and 116 to the Agaricomycetes. In addition, 6 microsporidia, 59 plant and 6 Opisthokonta(21) genomes were added, resulting in a database of 4,483 genomes. The database was divided into age categories ('phylostrata') based on the tree available at Mycocosm(10) and the eukaryotic tree published by Torruella et al.(21). The oldest phylostratum consisted of bacteria and archaea. Whole proteomes of *Coprinopsis cinerea*, *Armillaria ostoyae*, *Schizophyllum commune*, *Lentinus tigrinus*, *Phanerochaete chrysosporium* and *Rickenella mellea* were blasted against this database using mpiblast 1.6.0(22) with default settings. Blast hits were filtered with an E-value cut-off of $1x10^{-6}$ and a query coverage cut-off of 80%. After filtering, the age of each gene was defined as the node of the tree representing the last common ancestor of the species sharing homologs of the gene, at the specified blast cutoff.

To infer what Agaricomycete-specific genes are preferentially developmentally regulated, we analyzed the enrichment of annotation terms among developmentally regulated genes specific to Agaricomycetes compared to developmentally regulated genes whose origin predates the Agaricomycetes. To this end, we divided the phylostratigraphy profiles into two groups, corresponding to genes that originated before and those that originated after the origin of mushroom-forming fungi (Phylostratum 18). We tested for significant enrichment of IPR domains (evalue < 1e-5) in developmentally regulated genes that originated within the Agaricomycetes, relative to the other group of more ancient developmentally regulated genes using Fisher's exact test ($P < 0.05$).

Analyses of gene duplication/loss histories. The evolutionary history of 292 clusters containing developmentally regulated genes from 5 or 6 species was analyzed using the COMPARE pipeline (23). As a control we chose 290 clusters containing the same 5 or 6 species but developmentally regulated genes from none or one species, to compare the dynamics of shared developmentally regulated genes to genome-wide gene family dynamics. Predicted protein sequences of 74 fungal genomes representing the major clades of the kingdom fungi were clustered using MCL as described above. Multiple sequence alignments were obtained by using MAFFT 7.407 (mafft-l-ins-i) (24). A species tree was inferred based on 230 clusters of single copy orthologues present in at least half of the species using the PTHREADS version of RAxML 8.1.2 (25) under the PROTGAMMAWAG model. We performed ML bootstrapping with 100 bootstrap replicates using the rapid hill climbing algorithm and a partitioned model. For developmentally regulated families, ambiguously aligned sites were trimmed using TrimAl 1.2 (26) and gene trees were estimated in RAxML 8.1.2 (25) under the PROTGAMMAWAG model of protein evolution with 100 ML bootstrap as above. The gene tree – species tree reconciliation analyses were conducted using Notung 2.9 (27) with the edge weight threshold set to 70%. COMPARE was run as described previously(28) and duplications/losses mapped onto the species tree.

CAZyme annotation. Genes encoding putative carbohydrate-active enzymes were annotated using the CAZy pipeline. BLAST and Hmmer searches were conducted against sequence libraries and HMM

profiles in the CAZy database(29) (http://www.cazy.org). Positive hits were validated manually and assigned a family and subfamily classification across Glycoside Hydrolase (GH), Carbohydrate Esterase (CE), Glycoside Transferase (GT), Polysaccharide Lyase (PL), Carbohydrate-Binding Module (CBM) and Auxiliary redox enzyme (AA) classes of the CAZy system(30). Activities were determined by BLAST searches against biochemically characterized subsets of the CAZy database.

Coexpression analysis. Developmentally regulated genes in each species were clustered into co-expression modules based on their expression dynamics by using the clustering method implemented in Short Time-series Expression Miner (STEM v. 1.3.11)(31,32). Default parameters were used, except minimum absolute expression change, which was set to 4. Functional annotations of modules were obtained by GO enrichment analyses in TopGO (see below). For a higher-level grouping of co-expression modules, we defined six categories corresponding to early and late expressed genes, cap, stipe and gill specific genes and a mixed category. Coexpression modules were placed in one of these categories if more than half of the module's members had the same tissue- or stage-specific expression peaks. Modules without stage or tissue specificity were grouped in the mixed category. The early expressed category included coexpression modules with expression peaks in H, P1 or P2 stages, while late module category consisted of modules with young fruiting body and fruiting body stage specific expression peaks. We functionally annotated the modules and higher categories using InterPro Scan v5.24-63.0.

To visualize the kinase expression network across various kinase groups and developmental stages, a co-expression network was generated using Cytoscape *v*3.6.1 based on pairwise Pearson correlation coefficients for kinase expression patterns in *Coprinopsis cinerea*. Pairwise Pearson correlations coefficients for each kinase gene pair were calculated and for the appropriate visualization a 0.825 cut-off was applied for network construction.

Functional annotations, GO and InterPro enrichment. Gene Ontology (GO) enrichment analyses were carried out for developmentally regulated genes. For this, we annotated genes with GO terms based on their InterPro domain contents. Analyses were performed using Fisher's exact test with threshold $P<0.05$ in the R package topGO. The parameter algorithm weighted01 was chosen. Heatmaps were created using the heatmap.2 function of the R package 'gplots'. Unsupervised cluster analysis with Pearson's distance calculation and averaged-linkage clustering was carried out on the FPKM values, and heatmaps was visualised using z-score normalization on the rows via the heatmap.2 function.

Prediction of glycosylphosphatidylinositol anchored proteins (GPI-Ap) for the six species was performed using the portable version of Pred-GPI(33). From the proteins with a predicted GPI-anchor, we excluded ones which had no extracellular signal sequence, as assessed by SignalP version 4.1(34). Prediction of Small Secreted Proteins (SSP) for the six species was performed using a modified version of the bioinformatic pipeline of Pellegrin et al.(35). Proteins shorter than 300 amino acids were subjected to signal peptide prediction in SignalP (version 4.1) with the option "eukaryotic". Extracellular localisation of these proteins was checked with WoLFPsort version 0.2(36) using the option "fungi". Proteins containing transmembrane helix not overlapping with the signal peptide were also excluded. Prediction of transmembrane helices was performed with TMHMM (version 2.0)(37). Finally, proteins containing a KDEL motif (Lys-Asp-Glu-Leu) in the C-terminal region (prosite accession "PS00014") responsible for retention in the endoplasmic reticulum (ER) lumen, were identified using PS-SCAN (http://www.hpa-bioinfotools.org.uk/cgi-bin/ps_scan/ps_scanCGI.pl) and excluded.

We identified transcription factors based on the presence of InterPro domains with sequence-specific DNA-binding activity retrieved from literature data(38, 39) and manual curation of the Interpro-database. Annotated genes were then filtered based on their domain architecture in order to discard genes encoding DNA-binding proteins with functions other than transcription regulation (such as DNA-repair, DNA-replication, translation, meiosis).

We extracted the putative kinase genes from the 6 species based on their InterPro domain composition, and manually curated the classical kinases by excluding domains which correspond to metabolism related kinases and other non-classical protein kinases. The set of proteins having kinase related domains (Dataset S12) were subjected to BLAST searches (*BLAST 2.7.1+*, E-value 0.001) against the kinome of *Coprinopsis cinerea*(40) downloaded from Kinbase (www.kinase.com). The best hits for the six species were classified into eukaryotic protein kinase (ePK) and atypical protein kinases (aPK) and their families and subfamilies as described in the hierarchical kinase classification system(41).

Supplementary Note 1.

Co-expression clustering results. To address the question whether co-expressed genes responsible for developmental reprogramming during fruiting body formation can be identified, we performed STEM analysis. The number of co-expression modules was in strong correlation with the morphological complexity of fruiting bodies and the number of stages sampled: the more stages and tissue types a species had, the more co-expression modules were found. We categorized co-expression modules into 6 higher-ranked developmental categories, which we denote early, late, cap, stipe, gills and mixed modules. All or subsets of these were distinguished in each species, depending on the complexity of their fruiting bodies.

We distinguished 9 developmental stages and tissue types in *C. cinerea* and *A. ostoyae* both of which produce the most complex fruiting bodies among the six species. *Coprinopsis cinerea* had the largest number of developmentally regulated genes (7,475), which grouped into 40 co-expression modules and were classified into 6 modules (Table S1), while in *A. ostoyae* we found 4,417 developmentally regulated genes that grouped into 38 co-expression profiles and were categorized into 6 modules. In *L. tigrinus* we identified 8 developmental stages and tissue types and 1,862 developmentally regulated genes, which clustered into 30 co-expression modules and were classified into 5 modules. We determined 6 developmental stages and 6,427 developmentally regulated genes in *R. mellea* that grouped into 29 co-expression modules and were classified into 5 modules. In *S. commune,* which produces a simplified fruiting body without stipe, we distinguished only 5 developmental stages and found 2,000 developmentally regulated genes grouped into 27 co-expression modules and classified into 3 modules. Finally, in the corticioid *P. chrysosporium* we identified 3 developmental stages with altogether 753 developmentally regulated genes that were clustered into 11 co-expression profiles and categorized into 3 modules.

To determine the biological relevance of the co-expression profiles of each developmental module we performed GO enrichment analysis. Interestingly, expression maxima in the early module were not restricted to one stage but were spread out across multiple early stages. The GO terms enriched in the co-expression profiles of the early module included terms like constituent of cell wall, lipid metabolism, transmembrane transport, oxidation-reduction process, iron ion binding and transcription factor activity (Database S7). The enrichment of the functional terms oxidation-reduction processes and cell wall remodeling is consistent with the observations of the reduction of chitin contents in the hyphal knots compared to the vegetative hyphae(2,42). The importance of transcription factor activity during the early steps of fruiting body formation has been proven in *C. cinerea* (43) and *S. commune* (3).

The late developmental module includes genes with expression peaks in young fruiting body and fruiting body which were enriched in GO terms related to lipid metabolism, signaling, transmembrane transport, oxidation-reduction process, translation, tubulin, protease, isocitrate lyase, malate dehydrogenase, glutamate dehydrogenase and glutamate N-acetyltransferase (Database S13). These activities suggest an active role of the glyoxalate cycle, gluconeogenesis, and tricarboxylic acid pathways during late fruiting body development (2,44). Additionally, we found an overrepresentation of enzymes involved in the mobilization of glycogen reserves and nitrogen metabolism in *Coprinopsis* and *Armillaria*, both reported to have a role during cap expansion and stipe elongation (45). The enrichment of proteases has been reported from late stages in fruiting bodies of *C. cinerea* and *Agaricus bisporus* and the distantly related *Cordyceps sinensis* (2,46,47).

During the development of different tissue types, we found tissue-specific patterns of the overrepresented GO terms. The cap module includes genes with expression peaks both at pileal flesh and in the mixed tissue of pileal flesh and hymenium, from those species where these could not be separated. This category was enriched in replication, structural constituent of ribosome, amino acid transport, oxidation-reduction process, carbohydrate metabolism, cyanate metabolism, and glycogen phosphorylation related terms (Database S13). Some of these may be connected to the cellular uptake of water during cap expansion (2,45). The enrichment of cyanate metabolism related terms during cap development may be related to arginine biosynthesis that assist in a number of catalytic steps. The role of cyanate metabolism has been reported in the fruiting body formation and maturation of *Sordaria macrospor* (48,49), but has not been described in connection with the fruiting body development of Agaricomycetes so far. The gill module contains genes with expression peaks at the hymenium of *Coprinopsis* and *Armillaria*. This category was enriched in GO terms related to translation and ribosome biogenesis, which is the indicator of active protein synthesis (Database S13) that is consistent with the fact that this tissue hosts basidium and spore formation. The stipe module included genes with stipe specific expression peaks. This category was enriched in terms related to transmembrane transport, oxidation-reduction, constituent of cell wall, amino acid transmembrane transport, carbohydrate metabolism, and iron ion binding. The mixed module included genes without tissue or stage preference, therefore, this category was enriched in GO terms related to diverse processes (Database S13).

Shared functional signal in developmental modules across species. To gain a better insight into the biological processes underlying the development of different tissue types and developmental stages, we performed functional annotation by InterPro domains on the developmental modules in a species-wise manner and filtered out the domains shared by the majority of species. Each of the six species had early, late and mixed module categories. In these cases, the domain lists of 5- and 6-ways intersections were included in the analysis. Caps and stipes were distinguished in four species, while gills in two species. Therefore, the domain lists of 4-, 3-way intersection of cap modules and 2-ways intersections of stipe modules were included in the analysis.

In the early modules we found several domains shared by 5 or 6 species, such as dynamin, P-type ATPase, DEAD/DEAH box helicase, Pumilio RNA-binding, cytochrome P450, histone domains, cupin, and hydrophobin (Database S8) which are known to play a role in active membrane transport (50, 51), RNA metabolis (52), post-transcriptional regulation of gene expression (53), regulation of transcription, and hypothetically in cell adhesion (54).

In the late module category, aquaporin and thaumatin domains were shared by 5 or 6 species (Database S8). Aquaporins might be responsible for the transcellular water transport between adjacent cells that satisfy the increased demand of cellular water permeability of the developing fruiting body (55). Thaumatins have diverse functions, which are either related to their antifungal activity through

binding or hydrolyzing β-1,3-glucans of fungal cell walls, or play a role during maturation and senescence through some still unknown endogenous processes (56,57).

In the cap development module, cytochrome p450, glycoside hydrolase families, F-box, leucine-rich repeat, lectin, Zn(2)-C6 fungal-type DNA-binding, Homeobox, helicase and cyclin domains were shared by 3 or 4 species, which may play a role during carbohydrate metabolism, cell-cycle regulation, regulation of transcription, targeted protein degradation and oxidation-reduction processes (Database S14). These are consistent with the observations that the activity of glucosidase, protease and chitinase increase during the cap expansion in *C. cinerea* (2,45).

The cytochrome P450, F-box, leucine-rich repeat, BTB/POZ, protein kinase, major facilitator superfamily, glycoside hydrolases, carboxylesterase, glucose-methanol-cholin oxidoreductase, amino acid transporters, Armadillo-type fold, Homeobox and Zn(2)-C6 fungal-type DNA-binding protein domains were found in the stipe modules of 3 or 4 species (Database S14). These domains can be found in proteins playing a role in amino acid and carbohydrate transport, carbohydrate metabolism, regulation of transcription, targeted protein degradation, chromatin remodeling and signal transduction. Previous studies reported the role of chitin synthesis and cell wall remodeling during stipe formation, and the accumulation of glycogen at the base of stipe initial during early developmental steps, and the accumulation of trehalose and polyols as osmolytes during stipe elongation (2,45,58,59).

The gill module contains translation elongation factor EFTu-like, DNA mismatch repair protein MutS, transcription factor GTP binding and CBF/NF-Y/archaeal histone domains, ribosomal proteins (L7Ae, L30e, S12e, S26e, L12), protein argonaute, amino acid/polyamine transporter, glycoside hydrolase family 16 and 47, sugar transporter, hydrophobin, F-box, leucine-rich repeat, RING-type zinc finger and ubiquitin domains that are reported to be involved in processes such as DNA repair and replication, translation, ribosome biogenesis and targeted protein degradation.

The identification of modules of genes uniquely co-expressed in different stages and tissue-types gives a better insight into the fruiting body development of mushrooms. Based on these, we suggest that cell wall remodeling, carbohydrate and amino acid transport, targeted protein degradation and protein kinases may play a role in the development of the fruiting body. In addition to these, the post-transcriptional regulation of gene expression (Pumilio family proteins) can play an important role in the early steps of fruiting body formation as well. In the future, co-expression clustering and species and development module based assessments may shed the light on the molecular processes underlying fungal development in detail.

Table S1. Number of developmentally regulated genes, developmental stages, co-expression modules and the higher-ranked developmental categories of the six species.

	Dev.reg. Genes	Dev. Stages	Coexp. Modules	Dev. Categories
Coprinopsis	7475	9	40	6
Armillaria	4417	9	38	6
Lentinus	1862	8	30	5
Rickenella	6427	6	29	5
Schizophyllum	2000	5	27	3
Phanerochaete	753	3	11	3

Table S2. Conserved developmentally regulated (CAZyme) families and associated modules

Family	Activity	Putative FCW role/substrate	Conservation	Reports of role in development	Expansion in Agaricomycetes
AA1_1	Laccase	crosslinking	5 (P.chr.)	Several reports	$7.2x10^{-90}$
AA3_1	Cellobiose dehydrogenase	chitin	5 (L.tig)	Temp&Eggert 1990	$9.6x10^{-56}$
AA3_2/3	Glucose oxidase, aryl alcohol oxidase	H_2O_2 generation	6	This study	$<10^{-300}$
AA5_1/2	Glyoxal oxidase, galactose oxidase	H_2O_2 generation	6	This study	$2.2x10^{-3}$
AA9	Lytic polysaccharide monooxygenase	chitin	6	This study	$5.6x10^{-86}$
CBM1	Cellulose/chitin binding	chitin	5 (S.com.)	This study	n.s.
CBM12	Chitin binding	chitin	5 (P.chr.)	Sakamoto et al 2017	n.s.
CBM50	Chitin binding	chitin	5 (S.com.)	This study	$1.7x10^{-51}$
CE4	Chitooligosaccharide deacetylase	Chitin / chitosan	6	This study	$6.4x10^{-11}$
CE8	Pectin methylesterase	unknown	5 (C.cin.)	This study	n.s.
GH1_4	β-glucosidase	glucan	6	This study	n.s.
GH3_5	Exo-β-1,3-glucanase	glucan	5 (A.ost.)	This study	n.s.
GH5_7	Endo-β-1,4-mannanase	mannose	6	This study	$4.9x10^{-7}$
GH5_15	Endo-β-1,6-glucanase	glucan	5 (S.com.)	This study	$2.7x10^{-8}$
GH5_49, GH5_9	Endo-β-1,6-glucanase, exo-β-1,3-glucanase	glucan	6	Sakamoto et al 2017	$1.3x10^{-3}$
GH6	Exo-β-1,4-glucanase, cellobiohydrolase	glucan	5 (S.com.)	This study	n.s.
GH12_1	Endo-β-1,4-glucanase	glucan	5 (A.ost.)	This study	$2.6x10^{-3}$
GH16	Endo-β-1,3-1,4-glucanase	glucan	6	Sakamoto et al 2017	$1.2x10^{-26}$
GH16_2	Endo-β-1,3-glucanase, endo-β-1,3-1,4-glucanase	glucan	5 (L.tig)	This study	$1.2x10^{-26}$
GH17	Endo-β-1,3-glucanosyltransferase	glucan	6	This study	n.s.
GH18	Chitinase	chitin	5 (L.tig)	This study	$3.6x10^{-6}$
GH18_5	Chitinase	chitin	6	This study	$3.6x10^{-6}$
GH30_3	Endo-β-1,6-glucosidase	glucan	6	Sakamoto et al 2017	$2.7x10^{-14}$
GH71	Endo-β-1,3-glucanase	glucan	5 (P.chr.)	This study	$1.6x10^{-7}$
GH79_1	β-glucuronidase	unknown	4 (P.chr. S.com.)	This study	$1.7x10^{-52}$
GH92	□-1,3-mannosidase	mannose	5 (S.com.)	This study	$2.1x10^{-18}$
GH128	Endo-β-1,3-glucanase	glucan	5 (P.chr.)	Sakamoto et al 2017, 2011	n.s.
GH152	β-1,3-glucanase, thaumatin	glucan	6	This study	$2.0x10^{-18}$
PL5	Alginate lyase	?	6	This study	$9.17x10^{-04}$
PL14-like	Alginate lyase-like	?	6	This study	$8.5x10^{-19}$
Expansins	Cellulose/chitin loosening	chitin	6	Sipos et al 2017	$1.5x10^{-94}$
Kre9/Knh1	Glucan remodeling	glucan	6	Szeto et al 2007	$1.5x10^{-05}$

Only families that are developmentally regulated in 5 or 6 species are shown (except GH79). Conservation of the developmental regulation is given as the number of species in which a given family is developmentally regulated followed by the name(s) of species in which ther ewere no developmentally regulated members. Gene family expansion in the Agaricomycetes was tested by a Fisher exact test, and considered significant at $P < 0.05$. For the Kre9/Knh1 family, *P*-value refers to the overrepresentation of the corresponding InterPro domain.

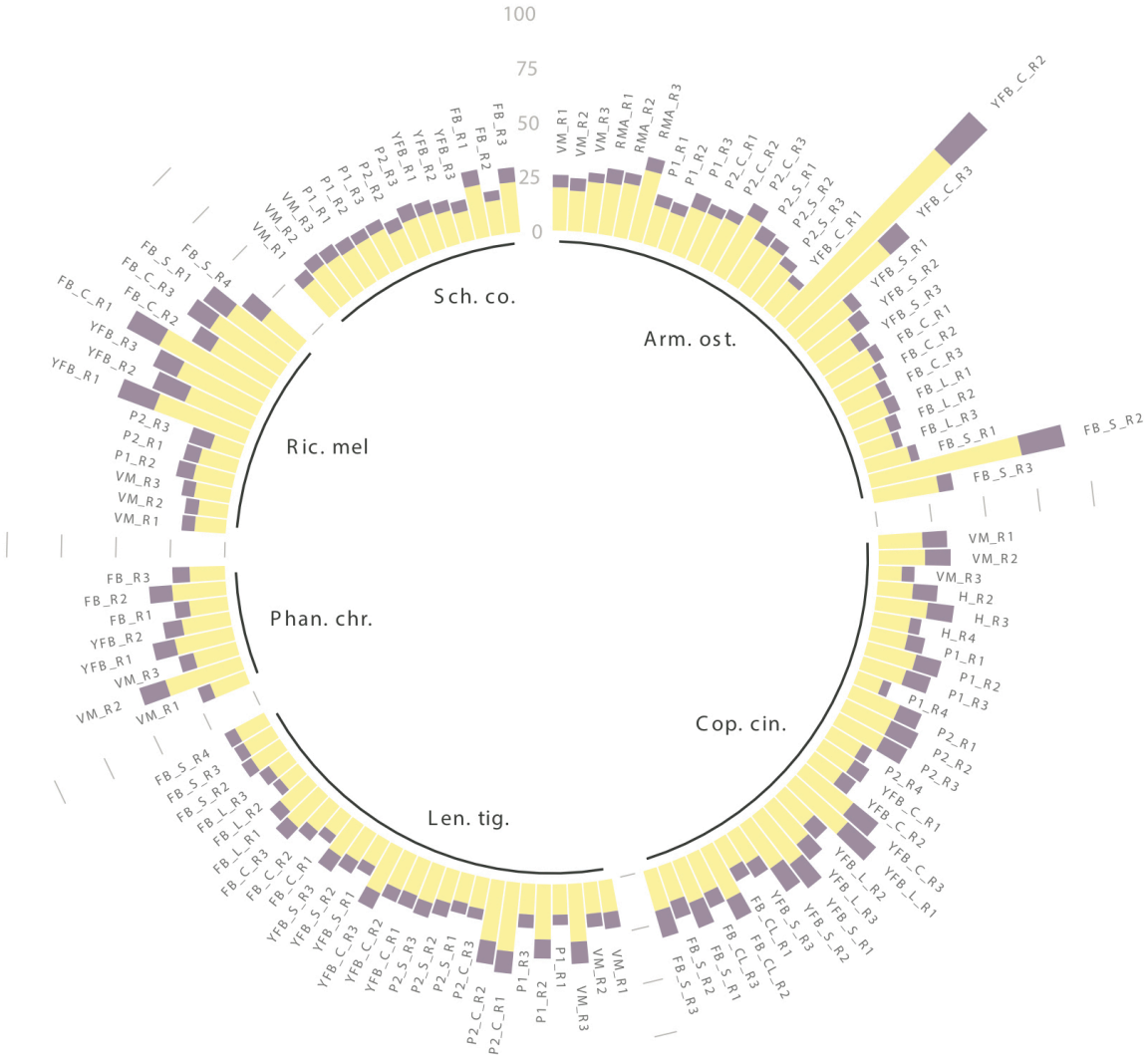

Fig. S1. Circular bar plot of RNA-Seq read mapping statistics for six species of Agaricomycetes. Bars are divided into properly mapped reads (yellow) and unmapped fragments (purple). Numbers are given in million read pairs. Abbreviations as follows: 'FB_S' fruiting body stipe; 'FB_L' fruiting body lamellae; 'FB_C' fruiting body cap; 'YFB_S' fruiting body stipe; 'YFB_L' fruiting body lamellae; 'YFB_C' fruiting body cap; 'P2' stage 2 primordium; 'P1' stage 1 primordium; 'H' secondary hyphal knot; 'VM' vegetative mycelium.

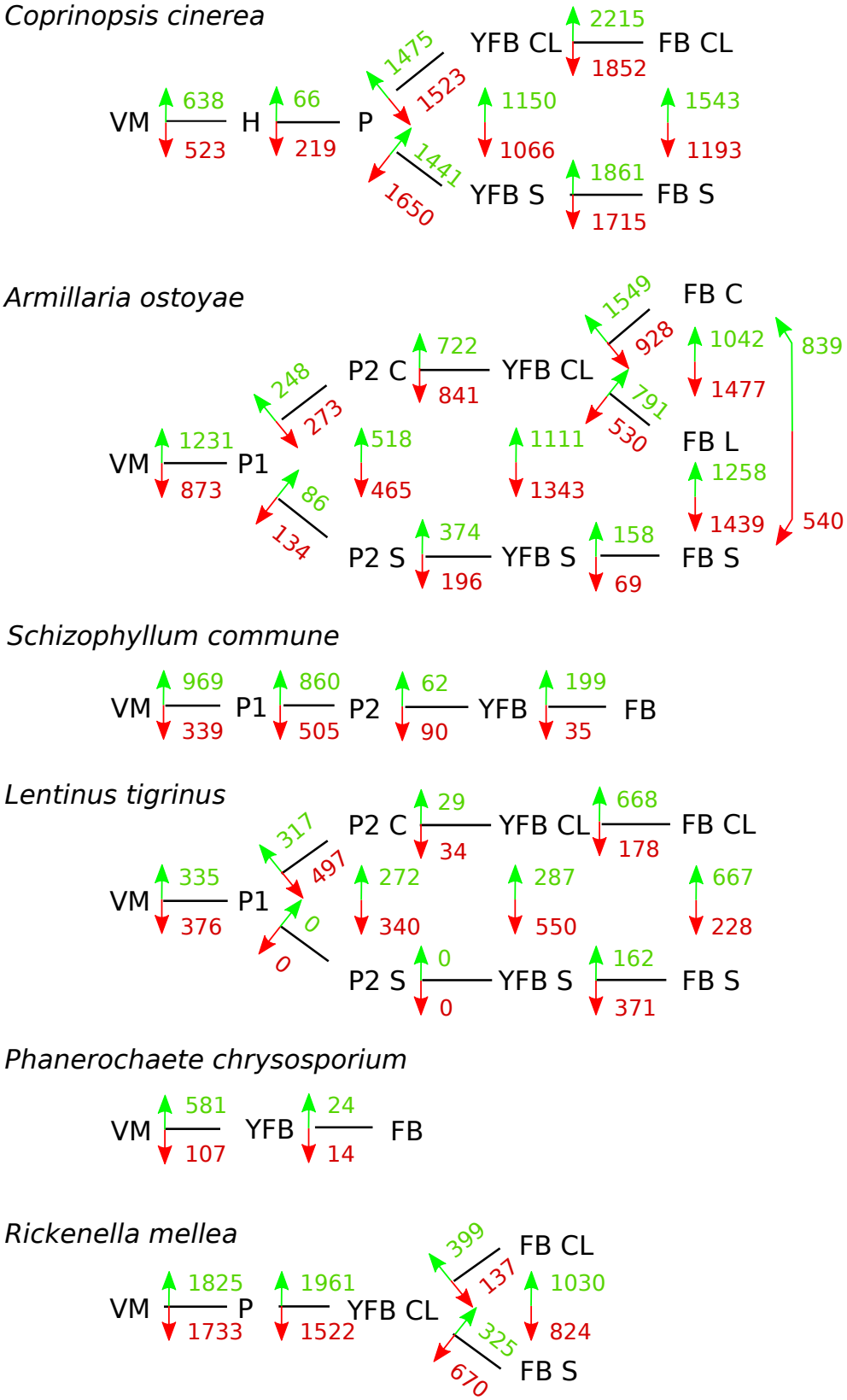

Fig. S2. Graphical representation of the number of significantly differentially expressed genes (DEG) among developmental stages and tissue types of six species of Agaricomycetes. Abbreviations: 'VM' vegetative mycelium; 'H' secondary hyphal knot; 'P1' stage 1 primordium; 'P2' stage 2 primordium; 'YFB' young fruiting body, 'FB' fruiting body; '_CL' cap and lamellae; '_S' stipe; '_L' lamellae.

Fig. S3. Wordcloud representation of enriched (P<0.05, Fisher exact test, Bonferroni correction) Gene Ontology terms among developmentally regulated genes of six species of Agaricomycetes. Font sizes are proportional to P-values.

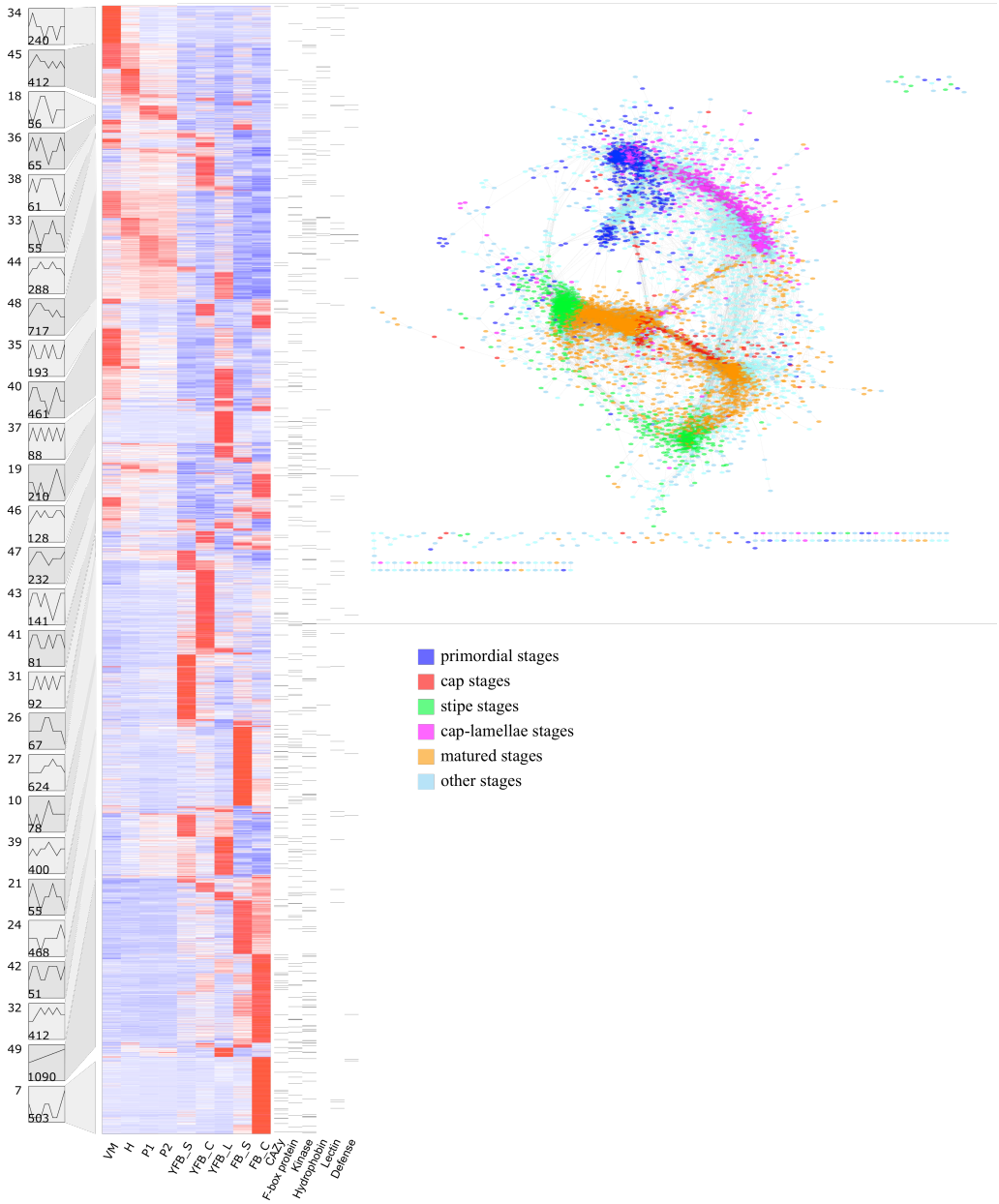

Fig. S4. Heatmap of developmentally regulated genes of *Coprinopsis cinerea*, with co-expression modules marked by expression profile logos. The number within the logo indicated the genes belonging to the module, the number next to it is the module ID. Only modules containing >50 genes are shown. Blocks of smaller modules are indicated by black line next to the heatmap. On the right, a co-expression network based on pairwise Pearson correlation coefficients of developmental gene expression is presented. Genes are colored by the genes' expression maxima. Abbreviations as follows: 'VM' vegetative mycelium; 'H' secondary hyphal knot; 'P1' stage 1 primordium; 'P2' stage 2 primordium; 'YFB' young fruiting body, 'FB' fruiting body; '_C' cap; '_L' lamellae; '_S' stipe.

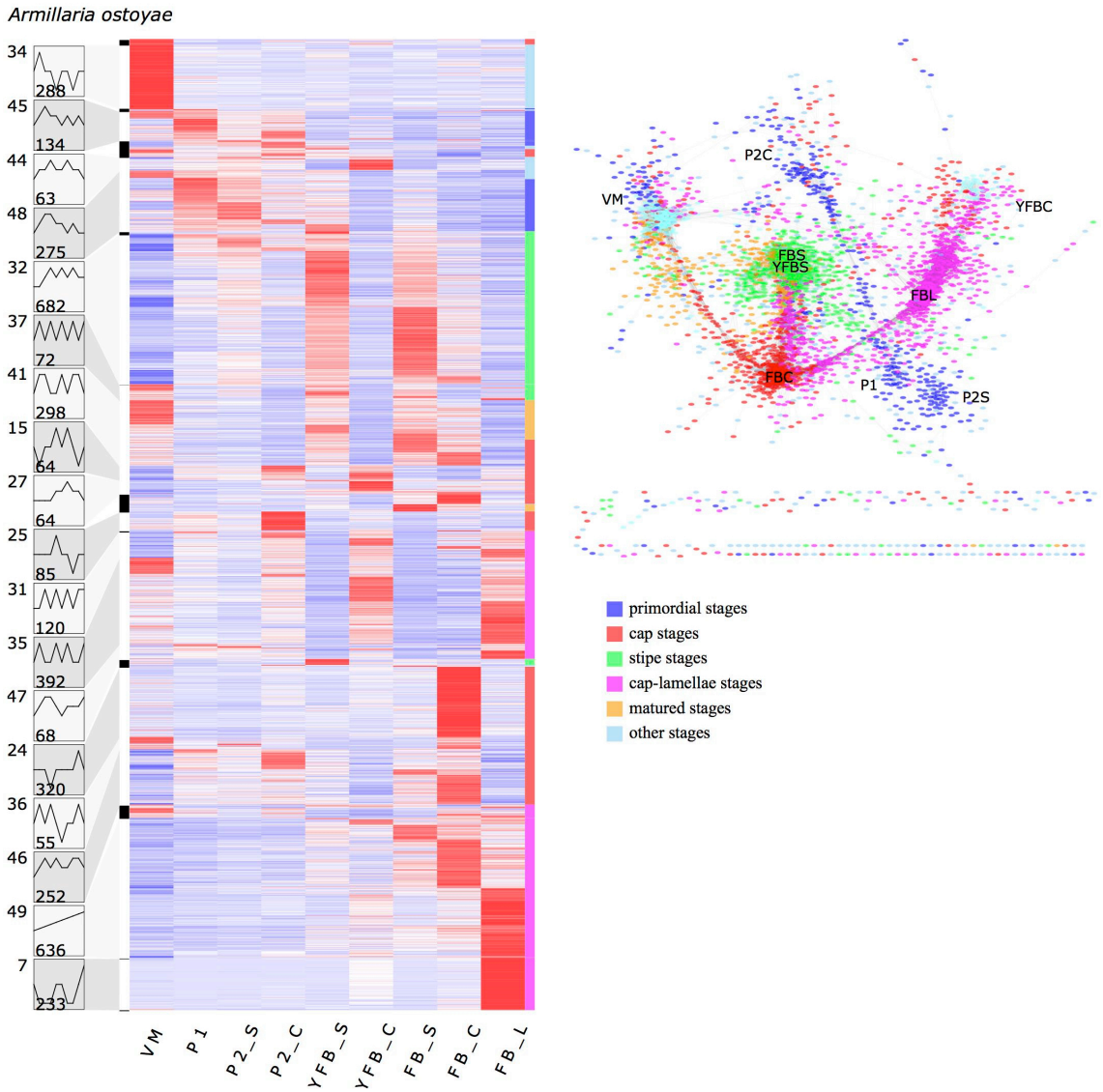

Fig. S5. Heatmap of developmentally regulated genes of *Armillaria ostoyae*, with co-expression modules marked by expression profile logos. The number within the logo indicated the genes belonging to the module, the number next to it is the module ID. Only modules containing >50 genes are shown. Blocks of smaller modules are indicated by black line next to the heatmap. On the right, a co-expression network based on pairwise Pearson correlation coefficients of developmental gene expression is presented. Genes are colored by the genes' expression maxima. Abbreviations as follows: 'VM' vegetative mycelium; 'P1' stage 1 primordium; 'P2' stage 2 primordium; 'YFB' young fruiting body, 'FB' fruiting body; '_C' cap; '_L' lamellae; '_S' stipe.

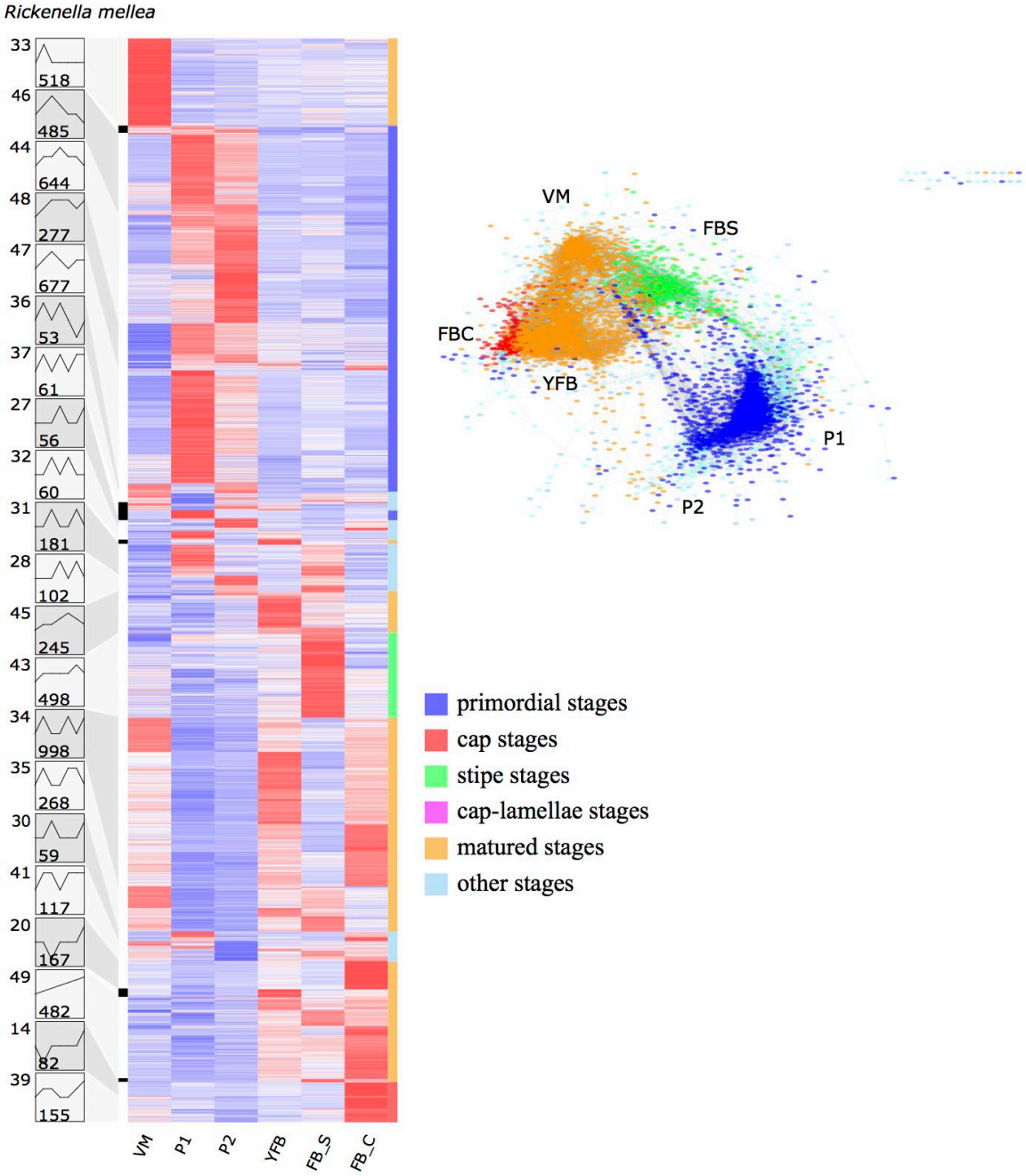

Fig. S6. Heatmap of developmentally regulated genes of *Rickenella mellea*, with co-expression modules marked by expression profile logos. The number within the logo indicated the genes belonging to the module, the number next to it is the module ID. Only modules containing >50 genes are shown. Blocks of smaller modules are indicated by black line next to the heatmap. Abbreviations as follows: 'VM' vegetative mycelium; 'P1' stage 1 primordium; 'P2' stage 2 primordium; 'YFB' young fruiting body, 'FB' fruiting body; '_C' cap; '_S' stipe.

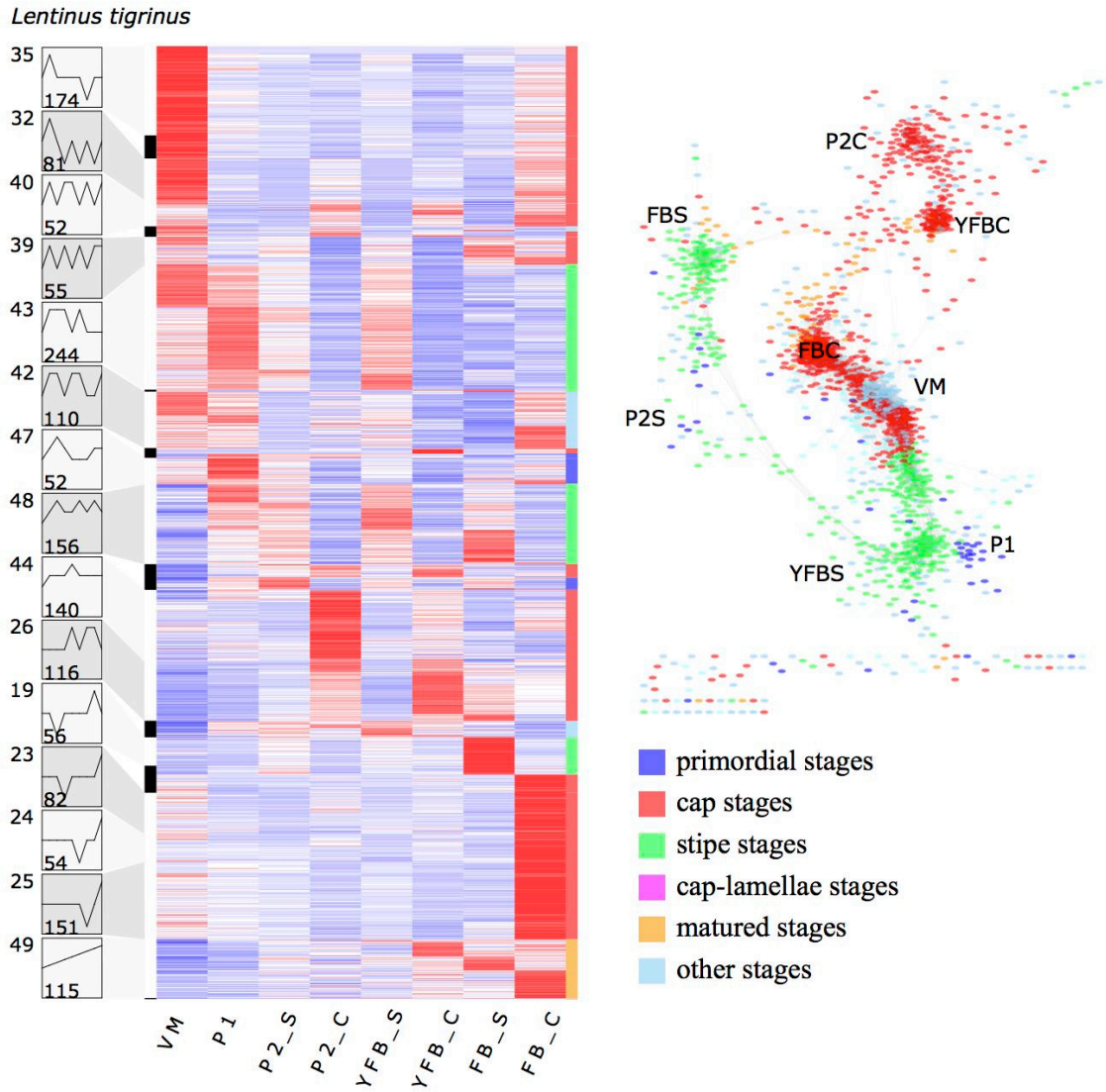

Fig. S7. Heatmap of developmentally regulated genes of *Lentinus tigrinus*, with co-expression modules marked by expression profile logos. The number within the logo indicated the genes belonging to the module, the number next to it is the module ID. Only modules containing >50 genes are shown. Blocks of smaller modules are indicated by black line next to the heatmap. Abbreviations as follows: 'VM' vegetative mycelium; 'P1' stage 1 primordium; 'P2' stage 2 primordium; 'YFB' young fruiting body, 'FB' fruiting body; '_C' cap; '_S' stipe.

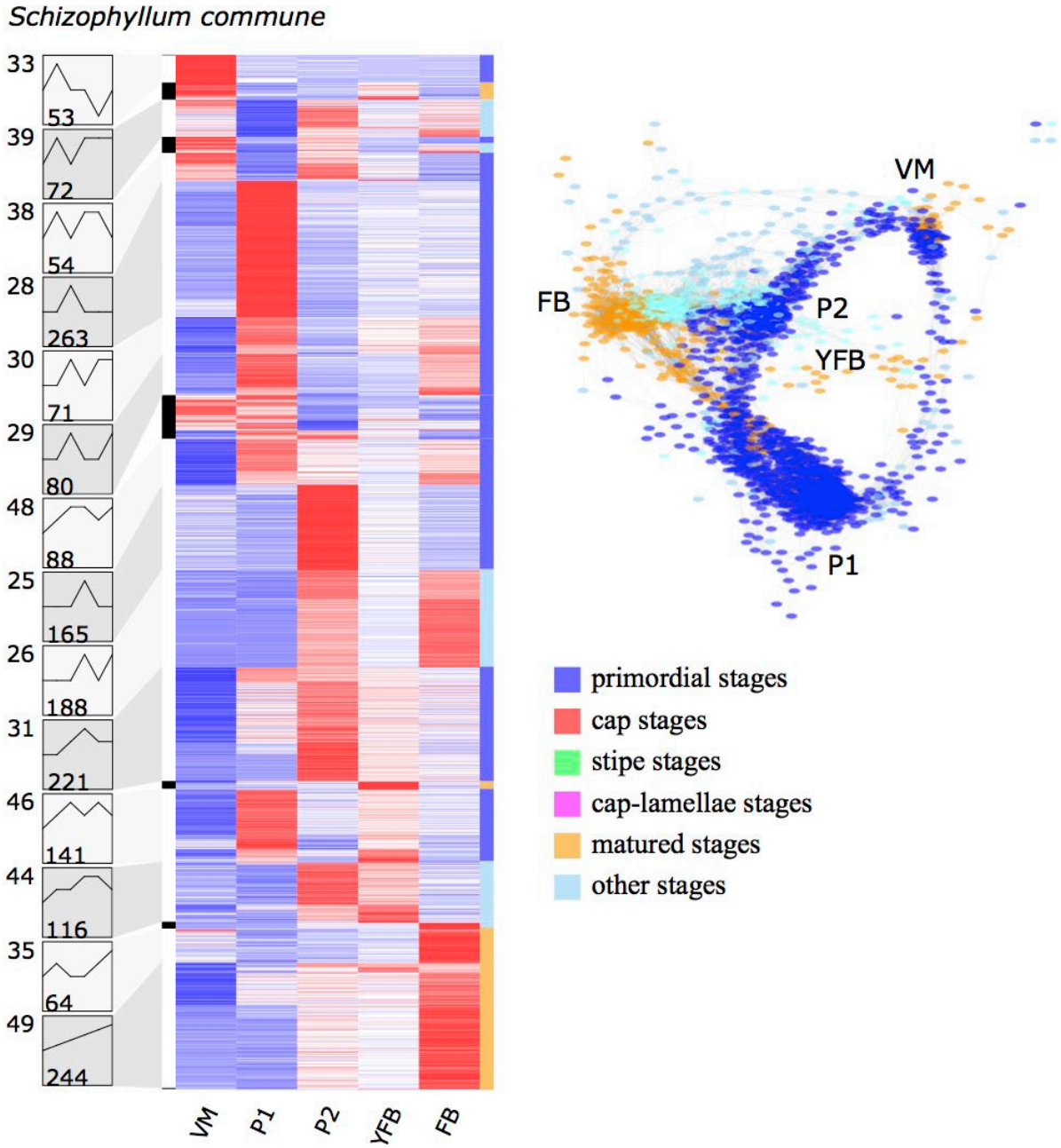

Fig. S8. Heatmap of developmentally regulated genes of *Schizophyllum commune*, with co-expression modules marked by expression profile logos. The number within the logo indicated the genes belonging to the module, the number next to it is the module ID. Only modules containing >50 genes are shown. Blocks of smaller modules are indicated by black line next to the heatmap. Abbreviations as follows: 'VM' vegetative mycelium; 'P1' stage 1 primordium; 'P2' stage 2 primordium; 'YFB' young fruiting body, 'FB' fruiting body.

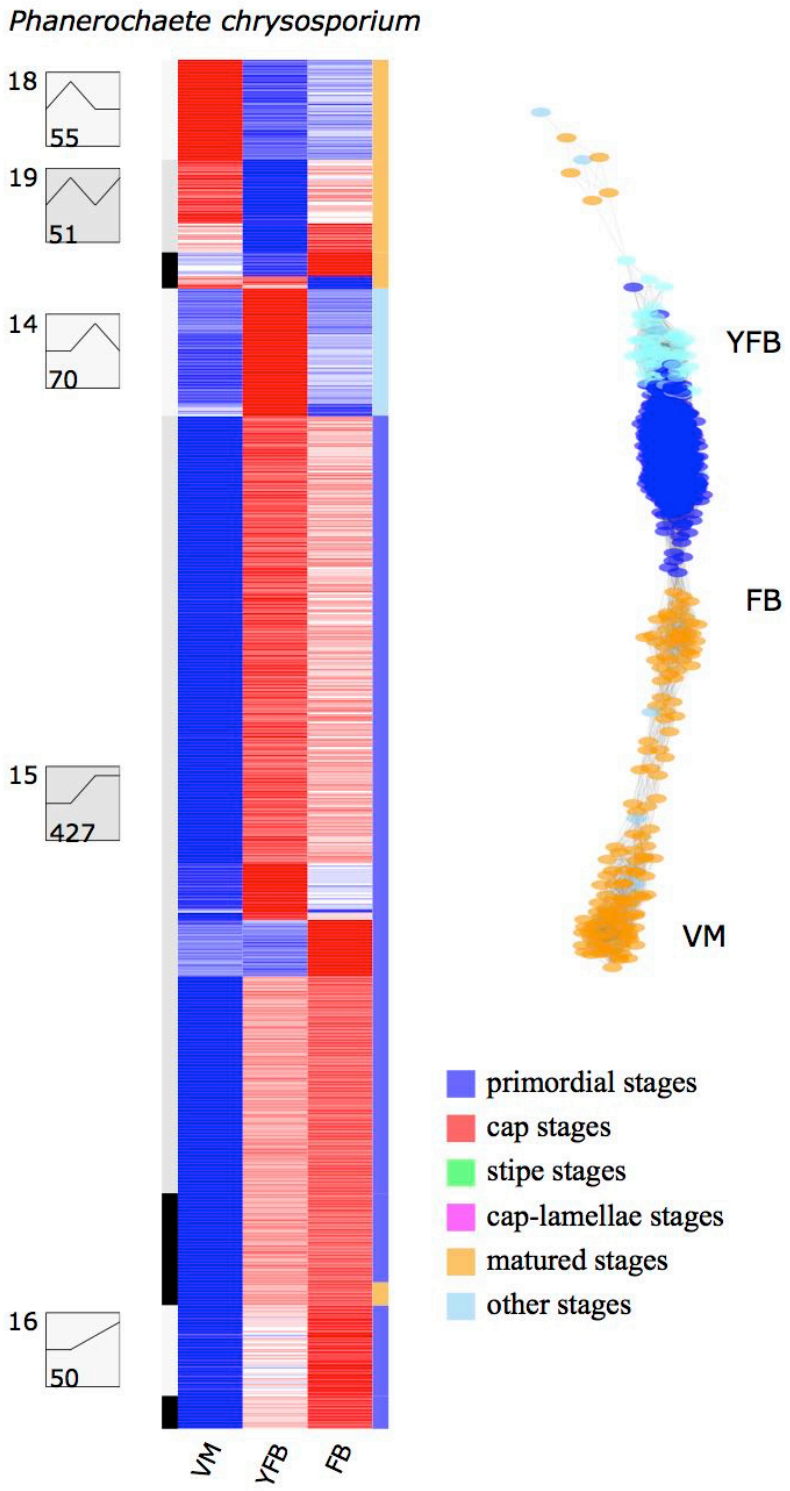

Fig. S9. Heatmap of developmentally regulated genes of *Phanerochaete chrysosporium*, with co-expression modules marked by expression profile logos. The number within the logo indicated the genes belonging to the module, the number next to it is the module ID. Only modules containing >50 genes are shown. Blocks of smaller modules are indicated by black line next to the heatmap. Abbreviations as follows: 'VM' vegetative mycelium; 'YFB' young fruiting body, 'FB' fruiting body.

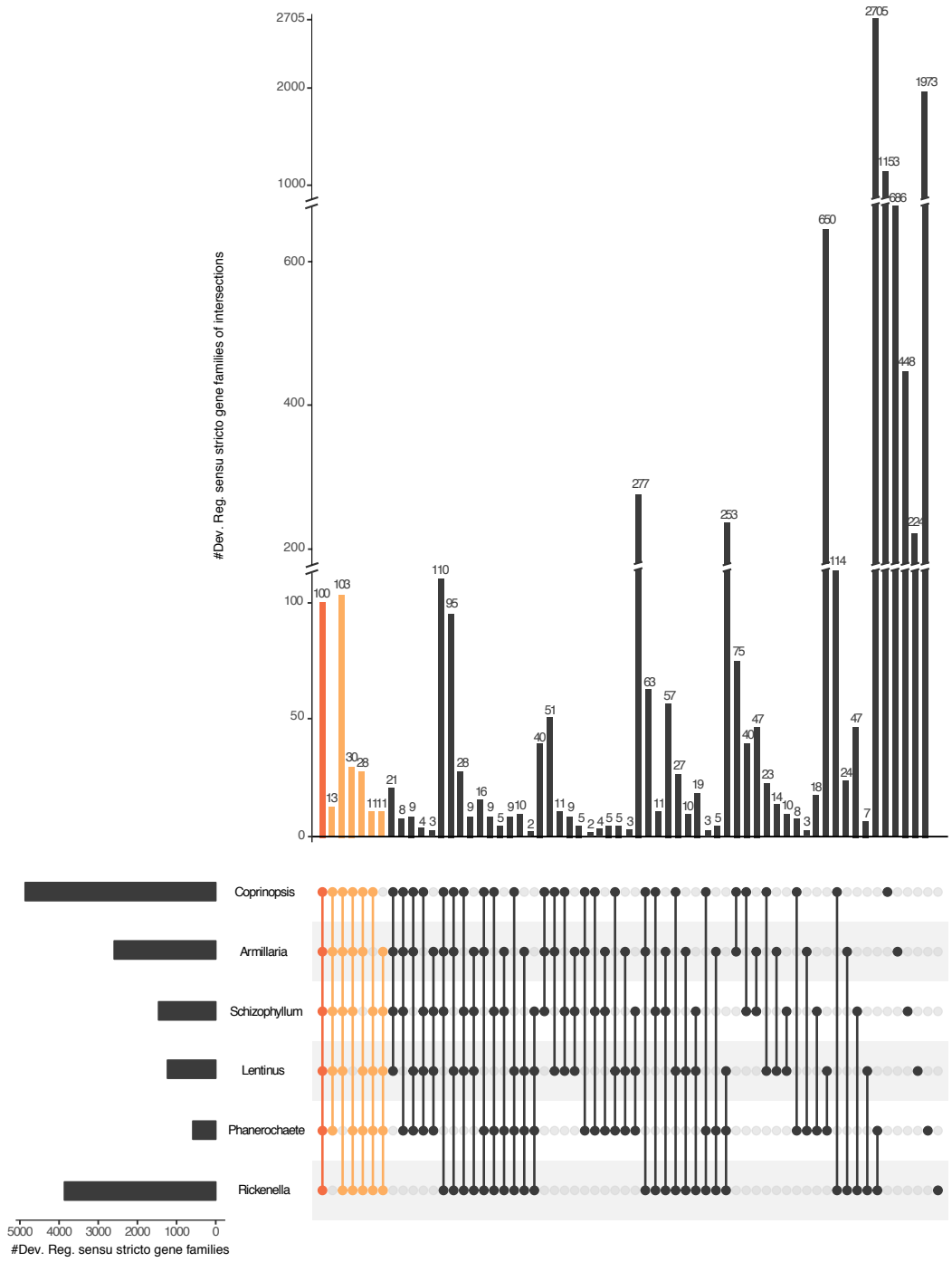

Fig. S10. UpSetR representation of developmentally regulated gene repertoires across six species of Agaricomycetes. Note that the number of species-specific genes were truncated for better visualization.

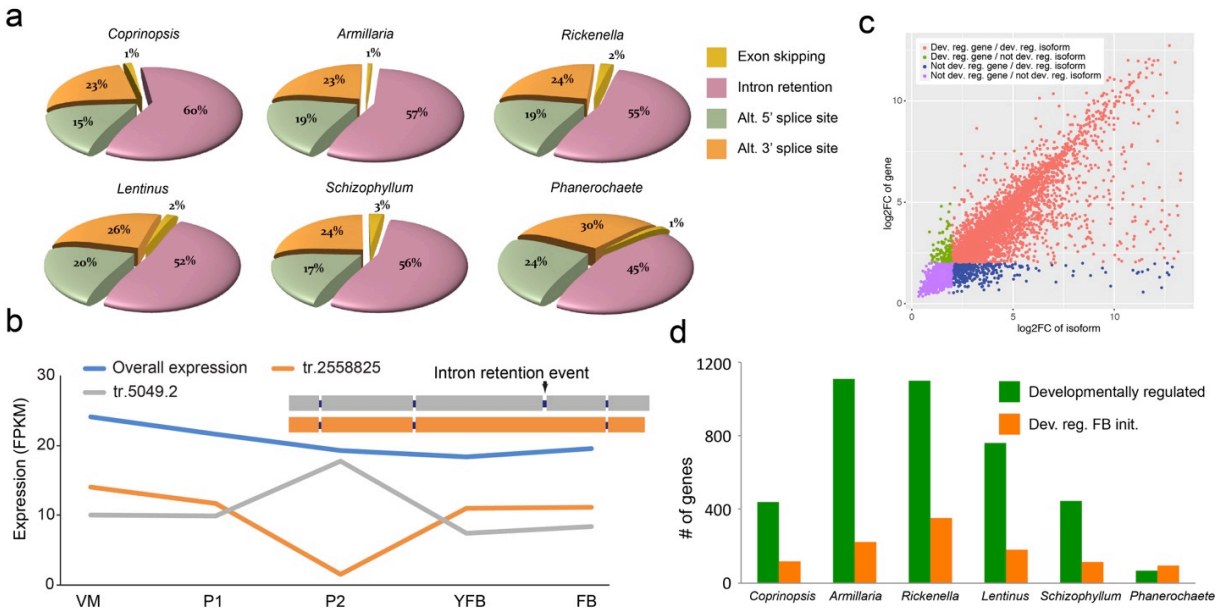

Fig. S11. Splicing patterns through fruiting body development. **a**. distribution of four main alternative splicing events across species (see also Dataset S9). **b**. Genes with little dynamics can contain developmentally regulated transcripts, Schco3_2558825 is shown here as an example. Abbreviations: VM - vegetative mycelium, P1 - stage 1 primordium, P2 - stage 2 primordium, YFB - young fruiting body, FB - mature fruiting body. **c**. Scatterplot of gene versus transcript expression dynamics in *Coprinopsis cinerea*, highlighting developmentally regulated transcripts (red). Plotted are fold change values between the minimum and maximum expression across all developmental stages for genes (y-axis) and alternative transcript (x-axis). Developmentally regulated transcripts (i.e. those that show FC>4 across any two developmental stages and FPKM>4) of non-developmentally regulated genes (FC<4) are highlighted in red. **d**. bar plot of developmentally regulated transcripts that were detected within not developmentally regulated genes.

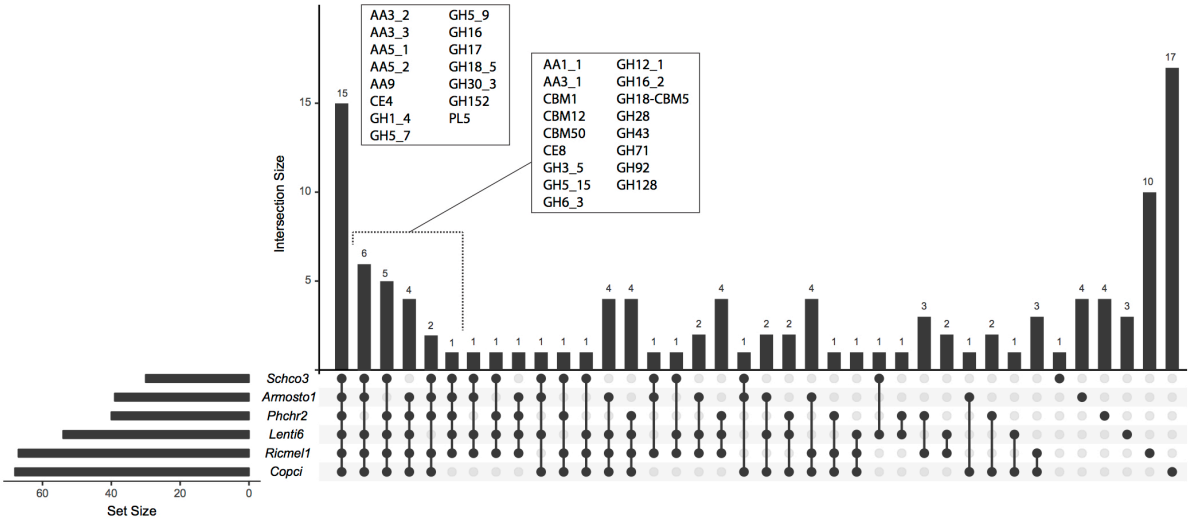

Fig. S12. UpSetR representation of developmentally regulated CAZyme repertoires across six species of Agaricomycetes. Families developmentally regulated in 6 and 5 are indicated.

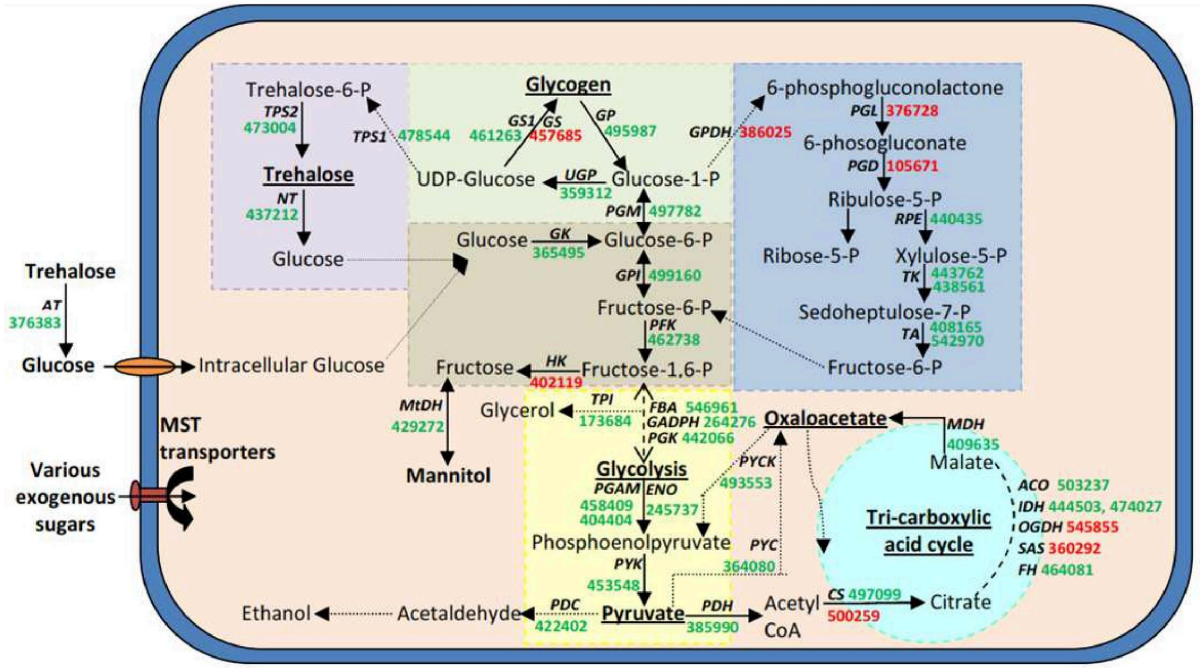
Trehalose-6-P
TPS2 473004
TPS1 478544
Trehalose
NT 437212
Glucose
Glycogen
GS1/GS 461263 457685
GP 495987
UDP-Glucose
UGP 359312
Glucose-1-P
PGM 497782
GPDH 386025
6-phosphogluconolactone
PGL 376728
6-phosogluconate
PGD 105671
Ribulose-5-P
RPE 440435
Ribose-5-P
Xylulose-5-P
TK 443762 438561
Sedoheptulose-7-P
TA 408165 542970
Fructose-6-P
Glucose GK 365495
GPI 499160
PFK 462738
Trehalose
AT 376383
Glucose
Intracellular Glucose
Fructose
HK 402119
Fructose-1,6-P
MtDH 429272
Mannitol
MST transporters
Various exogenous sugars
Glycerol
TPI 173684
FBA 546961
GADPH 264276
PGK 442066
Glycolysis
PGAM ENO 458409 404404 245737
Phosphoenolpyruvate
PYK 453548
PYCK 493553
PYC 364080
Oxaloacetate
MDH 409635
Malate
Tri-carboxylic acid cycle
ACO 503237
IDH 444503, 474027
OGDH 545855
SAS 360292
FH 464081
Ethanol
Acetaldehyde
PDC 422402
Pyruvate
PDH 385990
Acetyl CoA
CS 497099 500259
Citrate

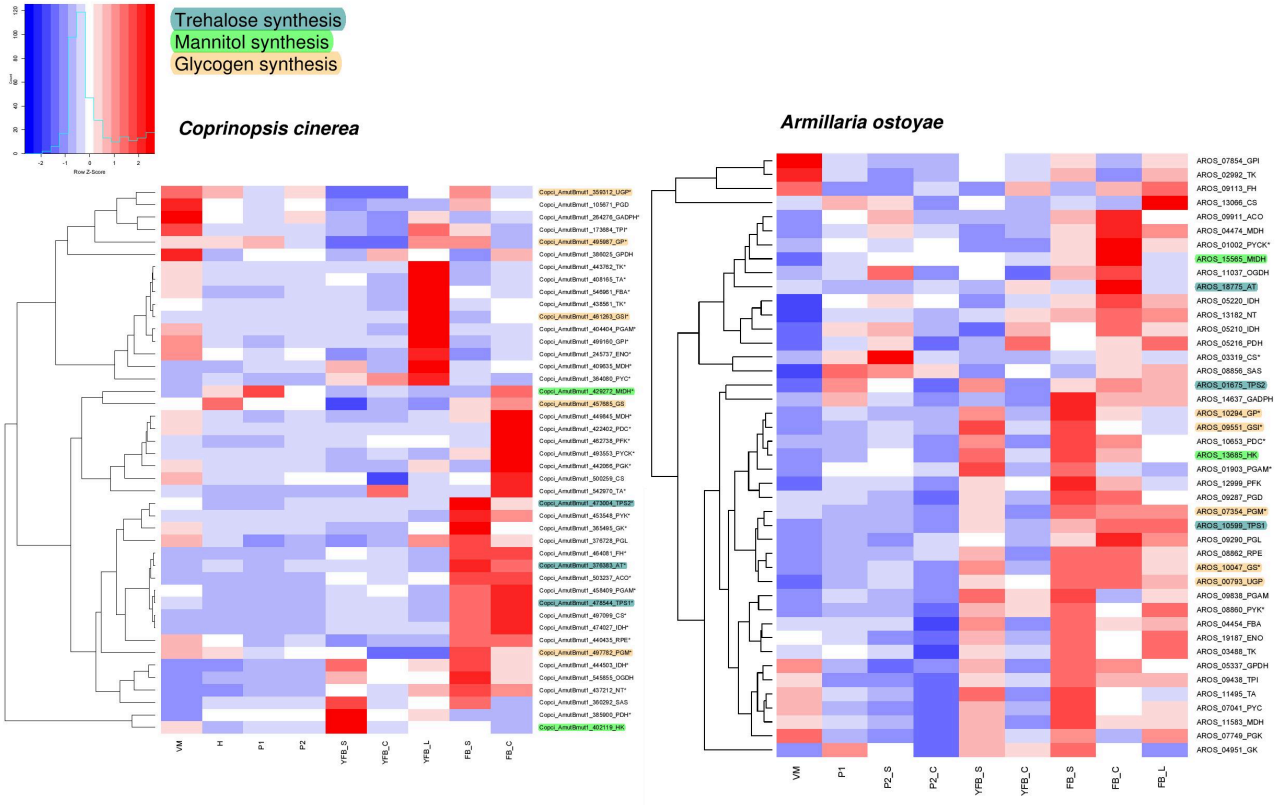
Trehalose synthesis
Mannitol synthesis
Glycogen synthesis
Coprinopsis cinerea
Armillaria ostoyae
VM
H
P1
P2
YFB_S
YFB_C
YFB_L
FB_S
FB_C
P2_S
P2_C

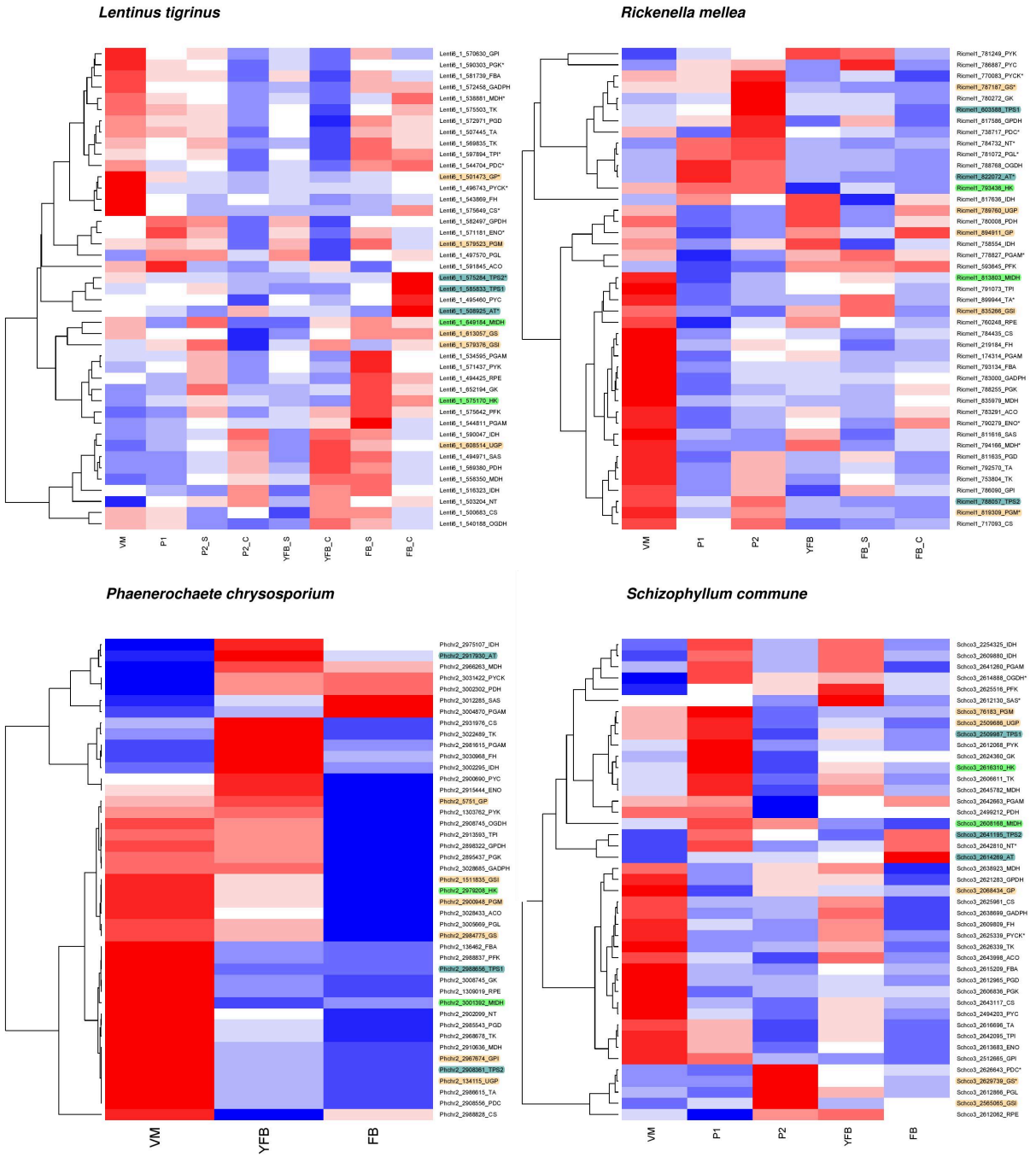

Fig. S13. Developmental regulation of primary carbohydrate metabolism in *Coprinopsis cinerea* (top) and the heatmap of primary carbohydrate metabolism related protein-encoding gene expression in the six species (bottom). Red and green font represent up- and downregulated genes, respectively. Abbreviations: 'VM' vegetative mycelium; 'H' secondary hyphal knot; 'P1' stage 1 primordium; 'P2' stage 2 primordium; 'YFB' young fruiting body, 'FB' fruiting body; '_CL' cap and lamellae; '_S' stipe; '_L' lamellae.

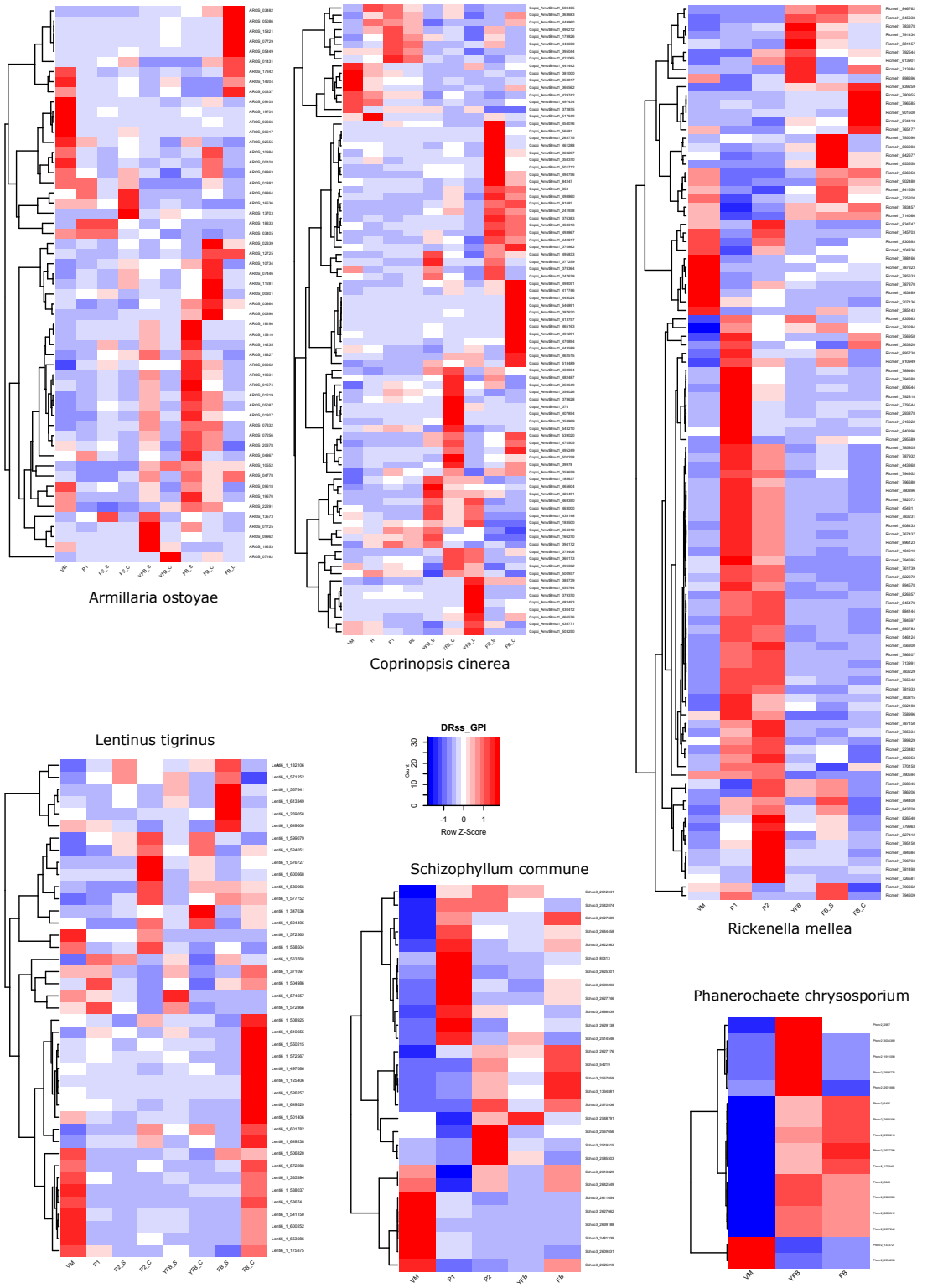

Fig. S14. Heatmaps of developmentally regulated GPI-anchored protein-encoding gene expression in six species of Agaricomycetes. Abbreviations: ‘VM’ vegetative mycelium; ‘H’ secondary hyphal knot; ‘P1’ stage 1 primordium; ‘P2’ stage 2 primordium; ‘YFB’ young fruiting body, ‘FB’ fruiting body; ‘_CL’ cap and lamellae; ‘_S’ stipe; ‘_L’ lamellae.

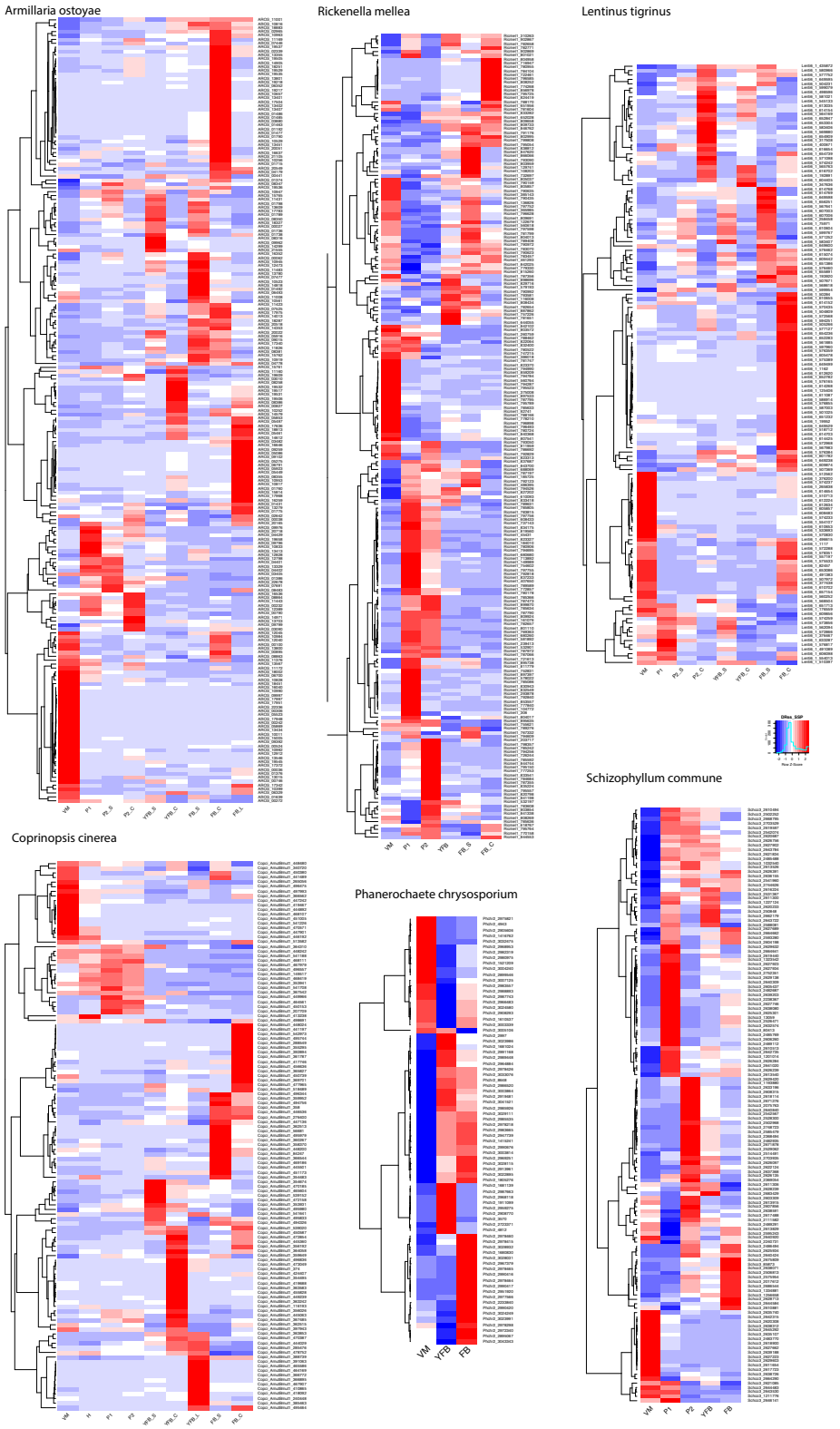

Fig. S15. Heatmaps of developmentally regulated SSP-encoding gene expression in six species of Agaricomycetes. Abbreviations: 'VM' vegetative mycelium; 'H' secondary hyphal knot; 'P1' stage 1 primordium; 'P2' stage 2 primordium; 'YFB' young fruiting body, 'FB' fruiting body; '_CL' cap and lamellae; '_S' stipe; '_L' lamellae.

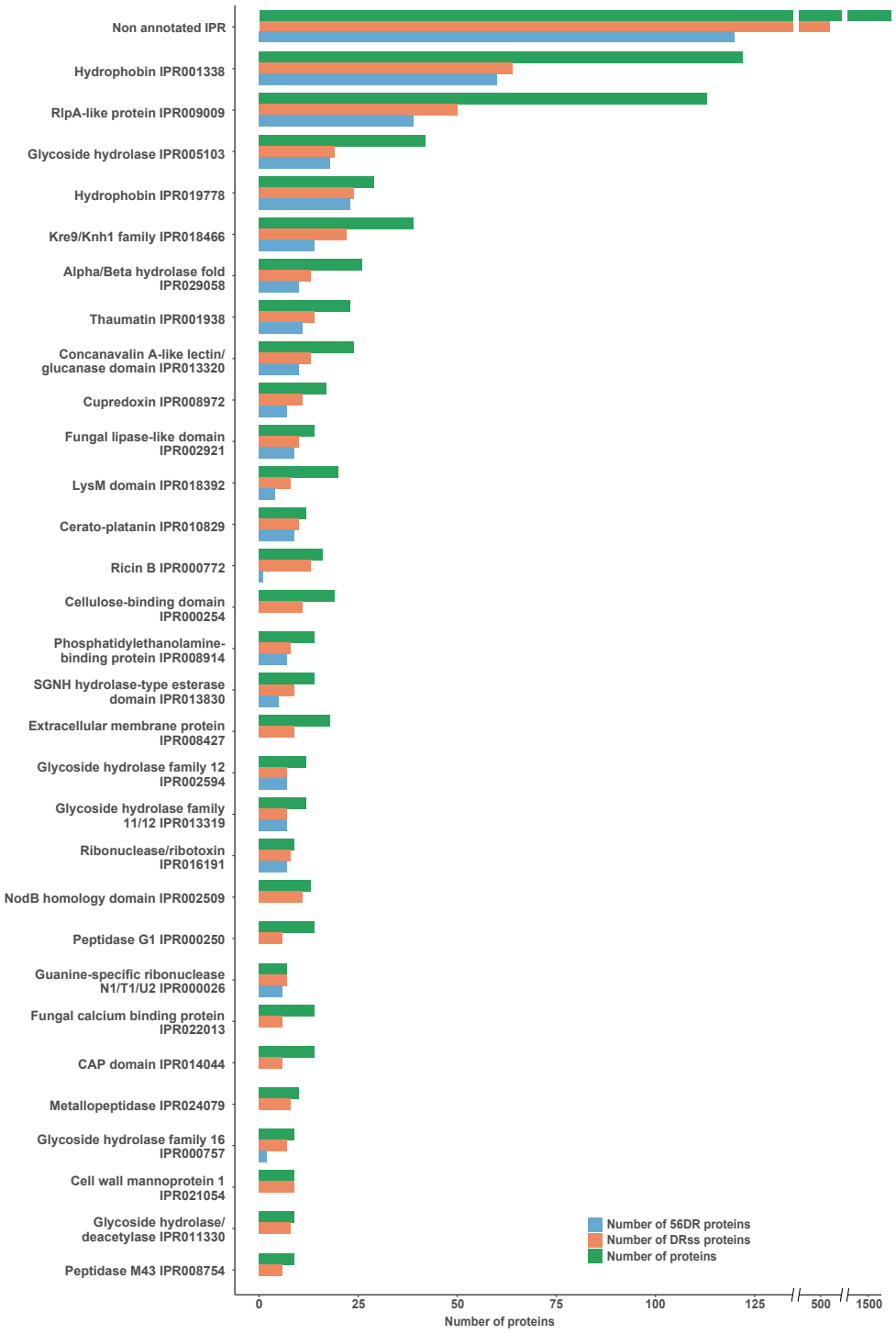

Fig. S16. Functional annotation of all (green bars), developmentally regulated (yellow bars) and conserved (in 5 or 6 species) developmentally regulated (blue bars) small secreted proteins across six species of Agaricomycetes.

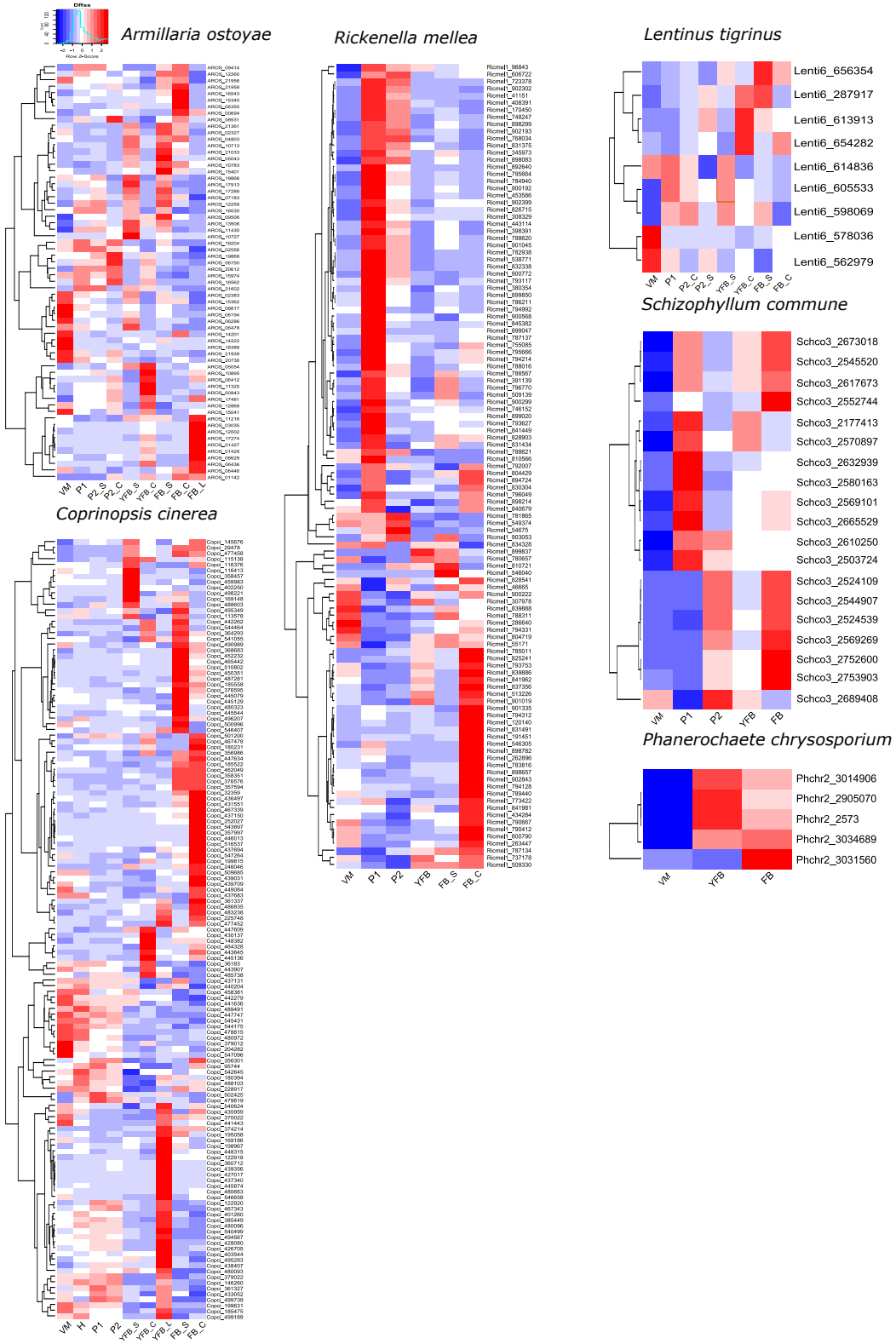

Fig. S17. Heatmaps of developmentally regulated F-box protein encoding gene expression in six species of Agaricomycetes. Abbreviations: 'VM' vegetative mycelium; 'H' secondary hyphal knot; 'P1' stage 1 primordium; 'P2' stage 2 primordium; 'YFB' young fruiting body, 'FB' fruiting body; '_CL' cap and lamellae; '_S' stipe; '_L' lamellae.

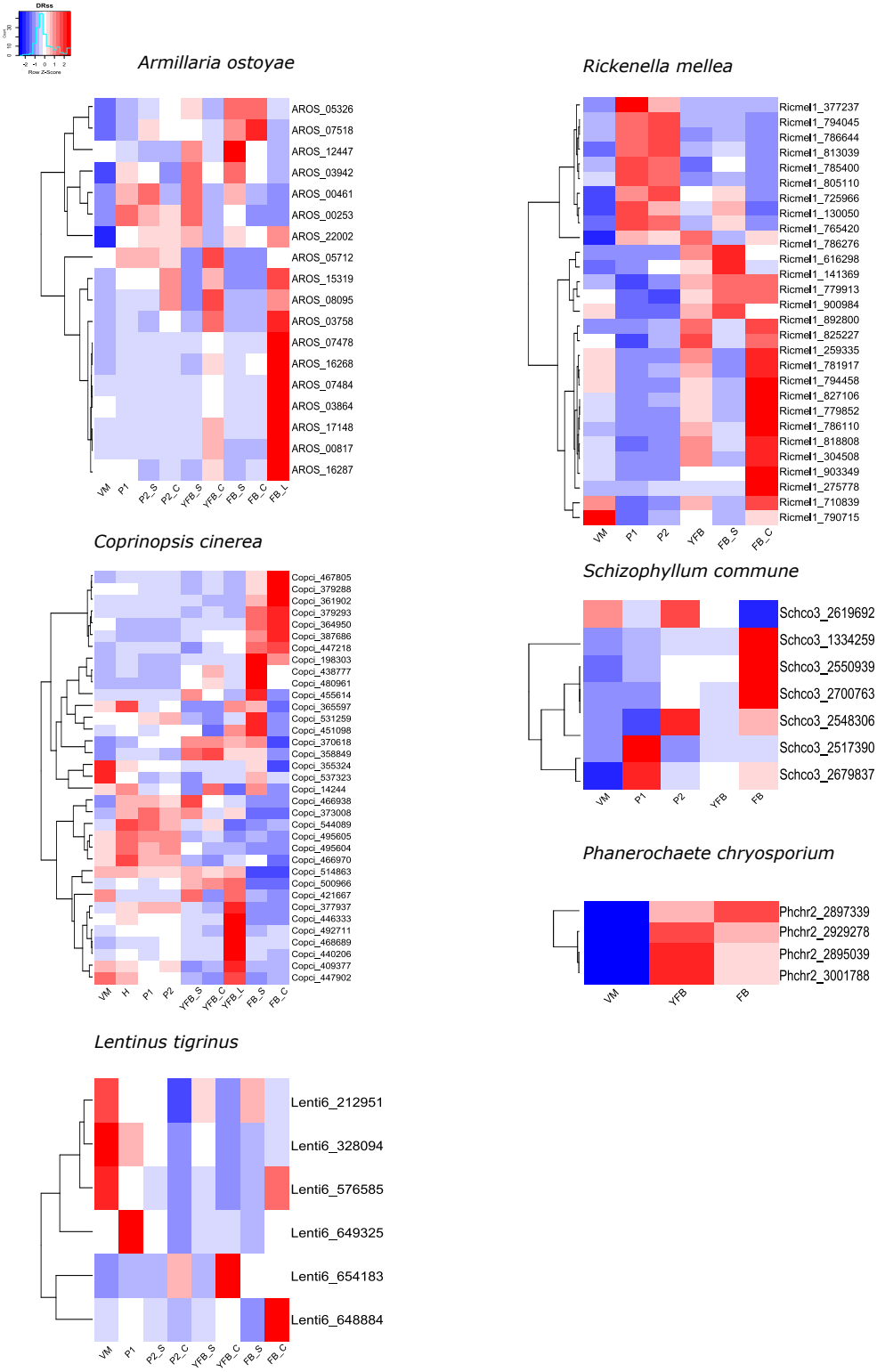

Fig. S18. Heatmaps of developmentally regulated RING-type Zinc finger domain containing gene expression in six species of Agaricomycetes. Abbreviations: 'VM' vegetative mycelium; 'H' secondary hyphal knot; 'P1' stage 1 primordium; 'P2' stage 2 primordium; 'YFB' young fruiting body, 'FB' fruiting body; '_CL' cap and lamellae; '_S' stipe; '_L' lamellae.

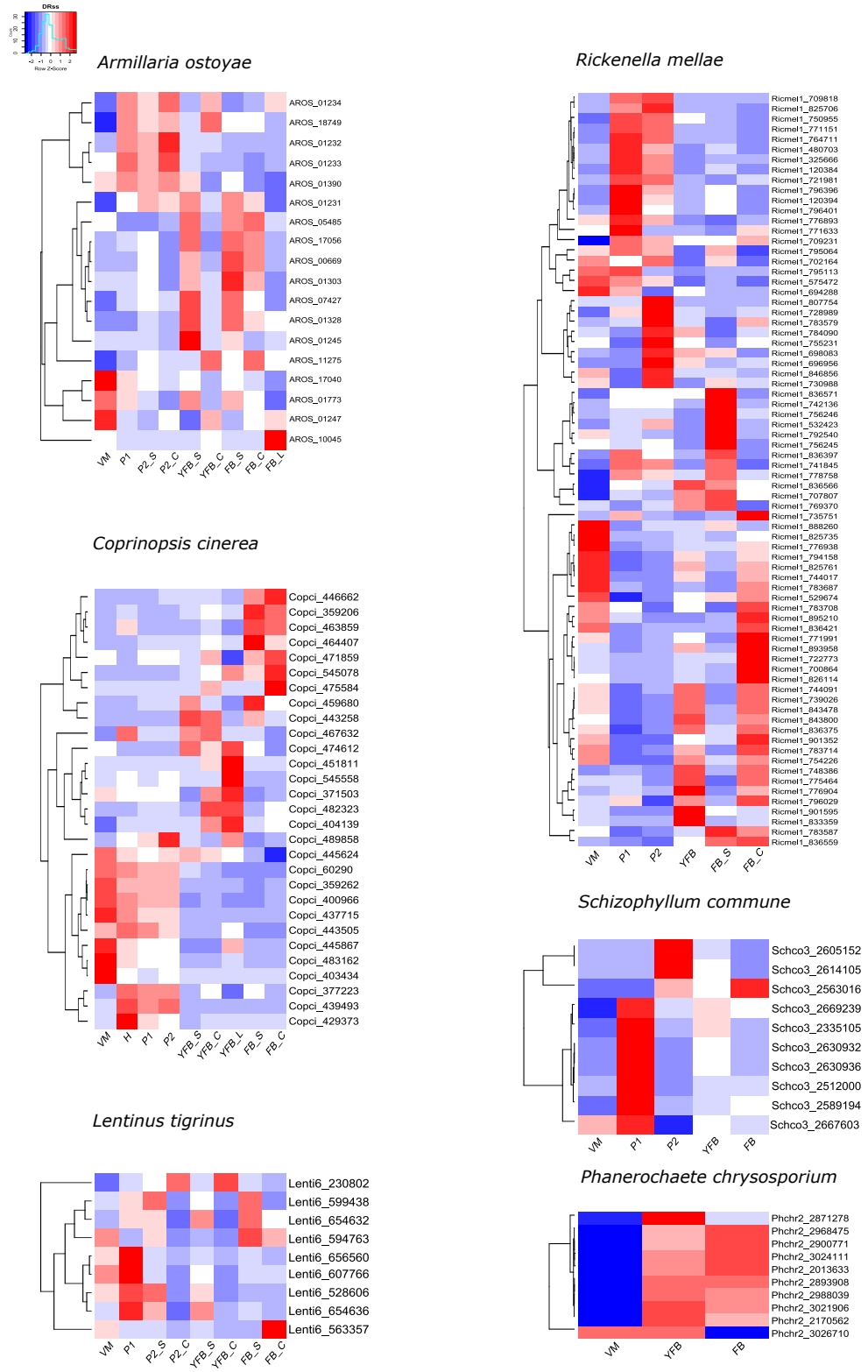

Fig. S19. Heatmaps of developmentally regulated BTB-POZ domain containing gene expression in six species of Agaricomycetes. Abbreviations: 'VM' vegetative mycelium; 'H' secondary hyphal knot; 'P1' stage 1 primordium; 'P2' stage 2 primordium; 'YFB' young fruiting body, 'FB' fruiting body; '_CL' cap and lamellae; '_S' stipe; '_L' lamellae.

a

Duplication context	*Coprinopsis*	*Armillaria*	*Rickenella*	*Lentinus*	*Schizophyllum*	*Phanerochaete*
Tandem	23.8	24.4	52.5	32.1	35.2	22.4
Segmental	2.6	7.1	3.4	3.2	5.2	0
Singleton	73.6	68.5	44.1	64.7	59.6	77.6

b

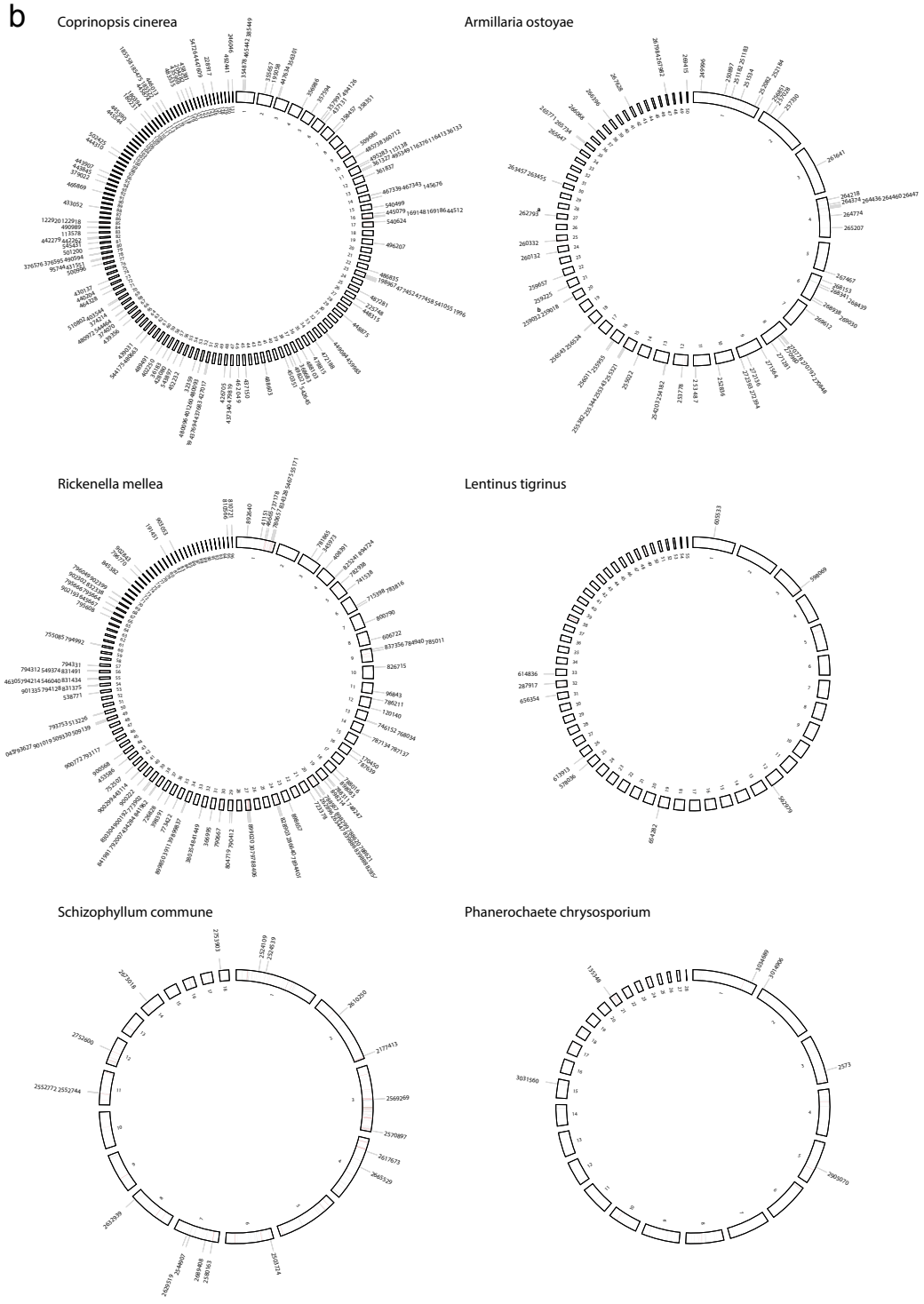

Fig. S20. (a) The context of gene duplications of F-box proteins in the genomes of six analyzed species. (b) Genomic context of F-box gene proliferation in six species of Agaricomycetes. Solid lines within the circus plot and indicated protein IDs mark F-box genes and developmentally regulated F-box genes, respectively.

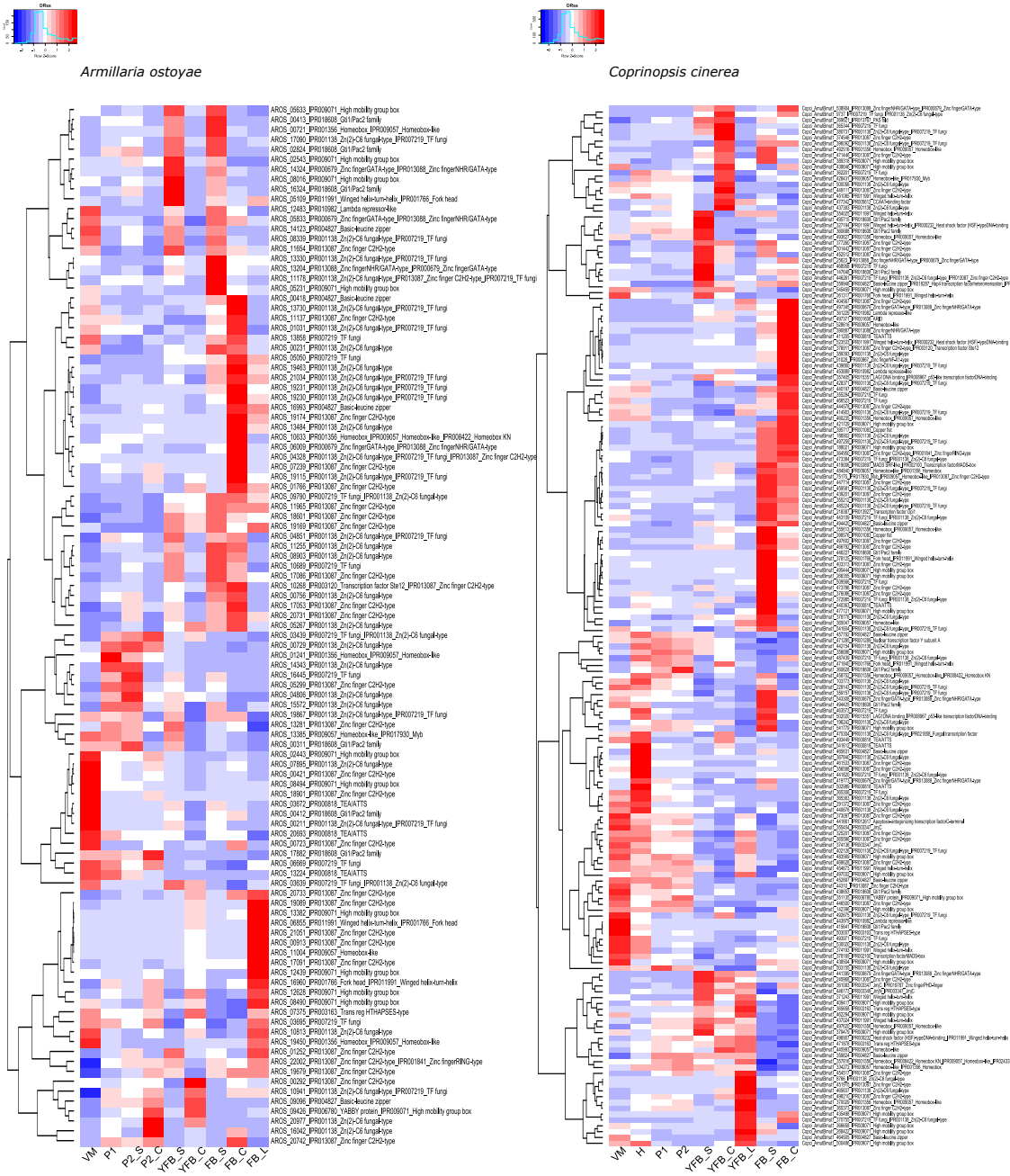

Fig. S21. Heatmaps of developmentally regulated transcription factor gene expression in six species of Agaricomycetes. Transcription factor family assignment is indicated in the protein IDs. Abbreviations: 'VM' vegetative mycelium; 'H' secondary hyphal knot; 'P1' stage 1 primordium; 'P2' stage 2 primordium; 'YFB' young fruiting body, 'FB' fruiting body; '_CL' cap and lamellae; '_S' stipe; '_L' lamellae.

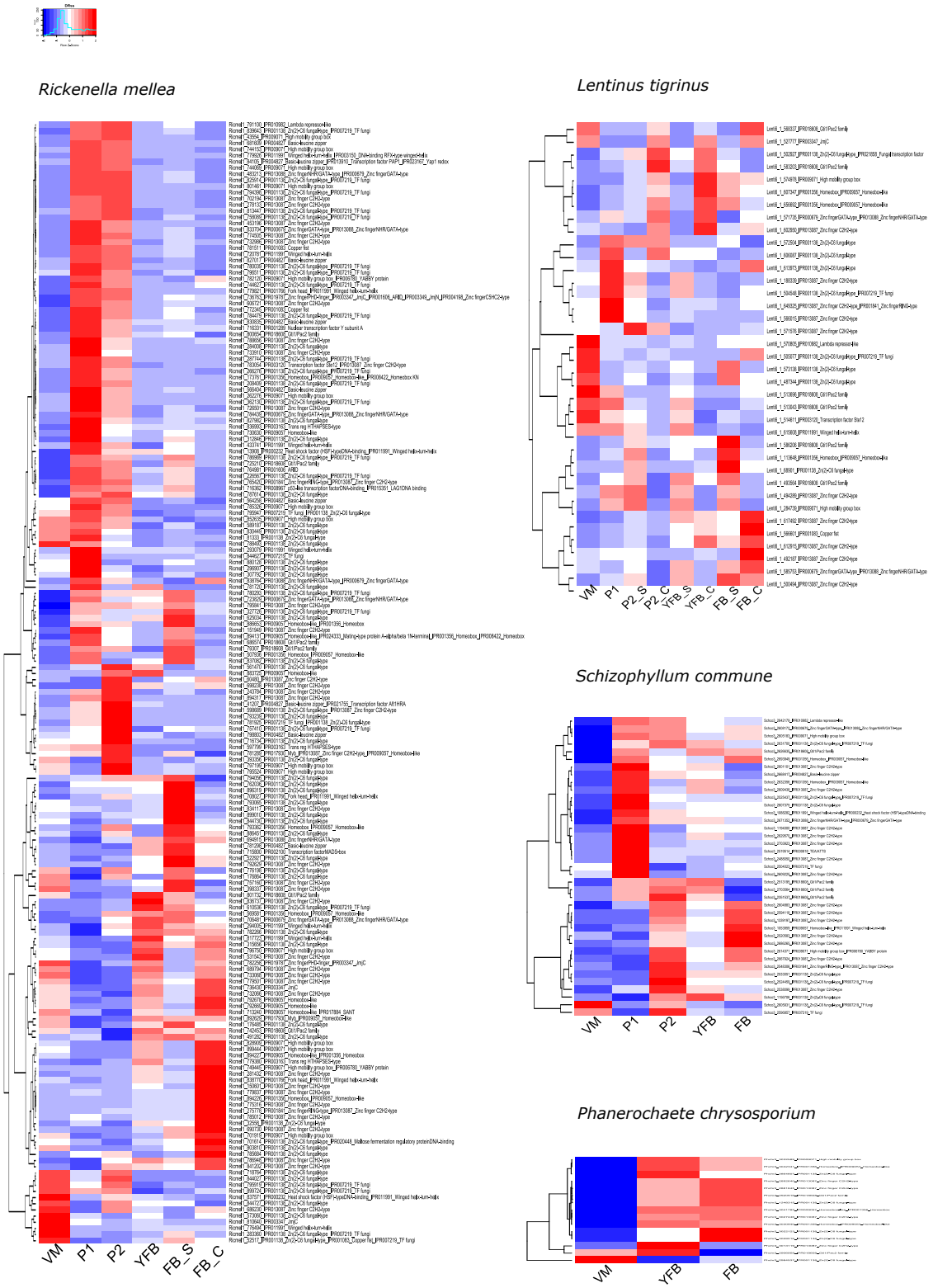

Fig. S22. Heatmaps of developmentally regulated transcription factor gene expression in six species of Agaricomycetes. Transcription factor family assignment is indicated in the protein IDs. Abbreviations: 'VM' vegetative mycelium; 'P1' stage 1 primordium; 'P2' stage 2 primordium; 'YFB' young fruiting body, 'FB' fruiting body; '_CL' cap and lamellae; '_S' stipe; '_L' lamellae.

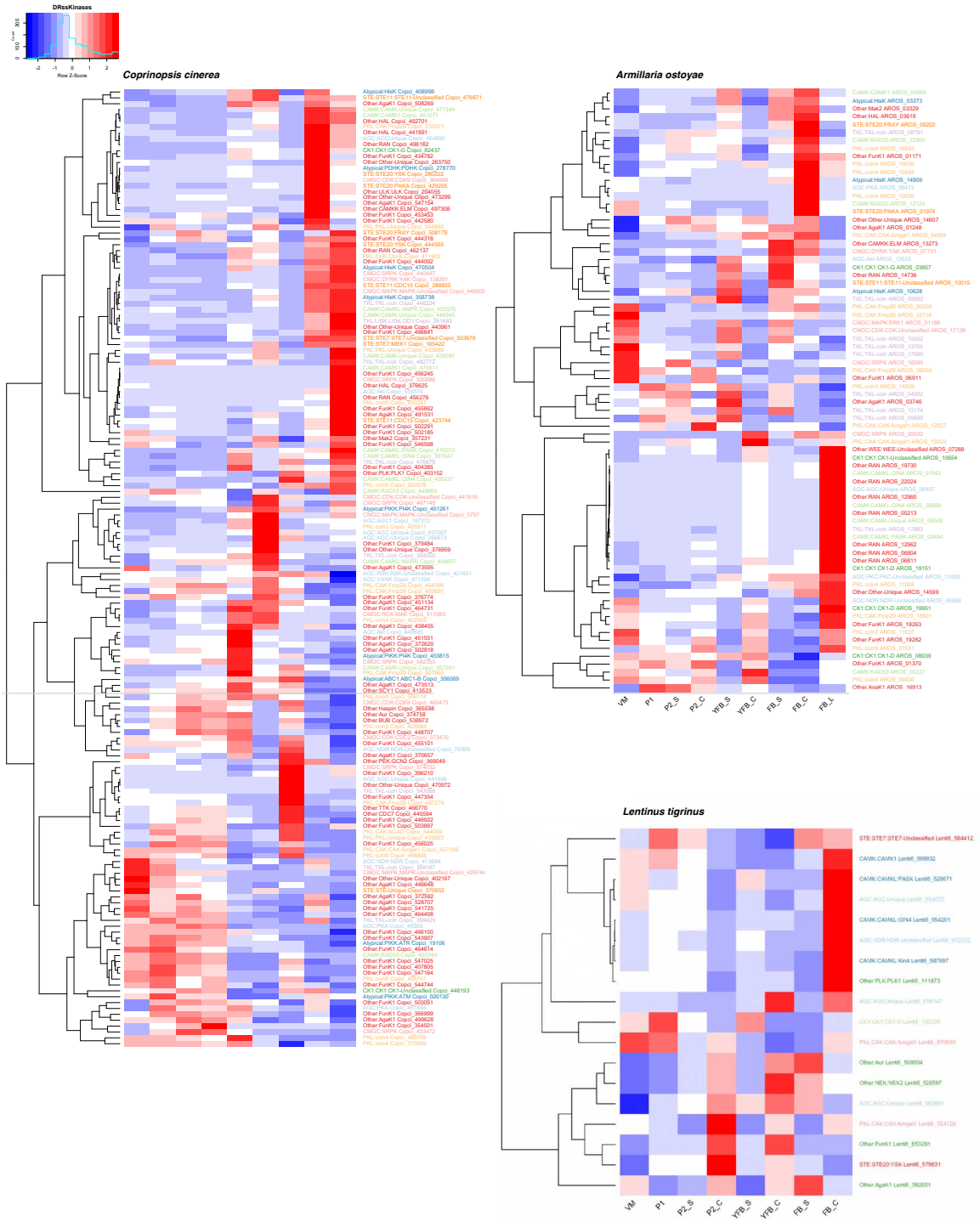

Fig. S23. Heatmaps of developmentally regulated kinases in six species of Agaricomycetes. Protein ID-s are colored by classification. Abbreviations: 'VM' vegetative mycelium; 'H' secondary hyphal knot; 'P1' stage 1 primordium; 'P2' stage 2 primordium; 'YFB' young fruiting body, 'FB' fruiting body; '_CL' cap and lamellae; '_S' stipe; '_L' lamellae.

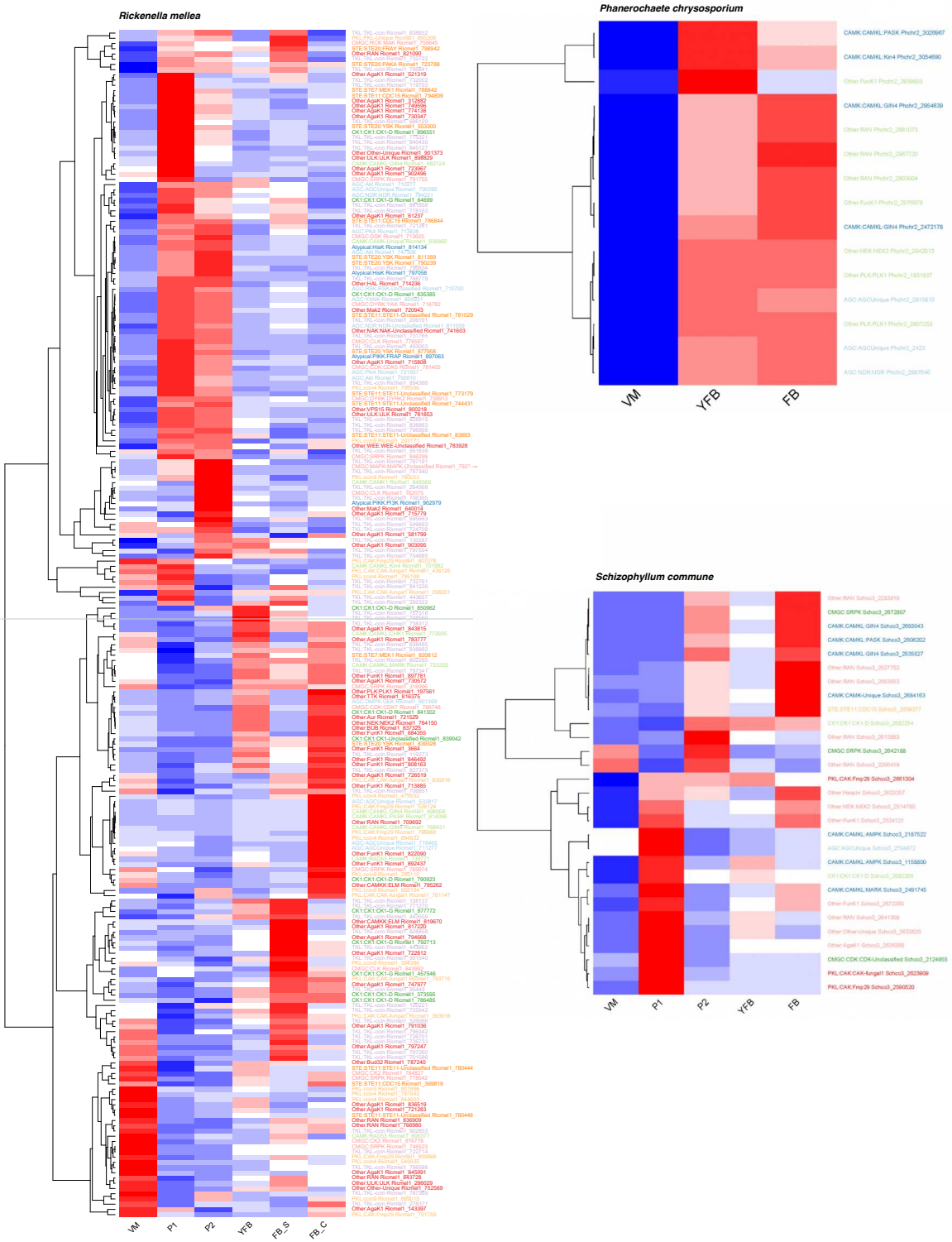

Fig. S24. Heatmaps of developmentally regulated kinases in six species of Agaricomycetes. Protein ID-s are colored by classification. Abbreviations: 'VM' vegetative mycelium; 'P1' stage 1 primordium; 'P2' stage 2 primordium; 'YFB' young fruiting body, 'FB' fruiting body; '_CL' cap and lamellae; '_S' stipe; '_L' lamellae.

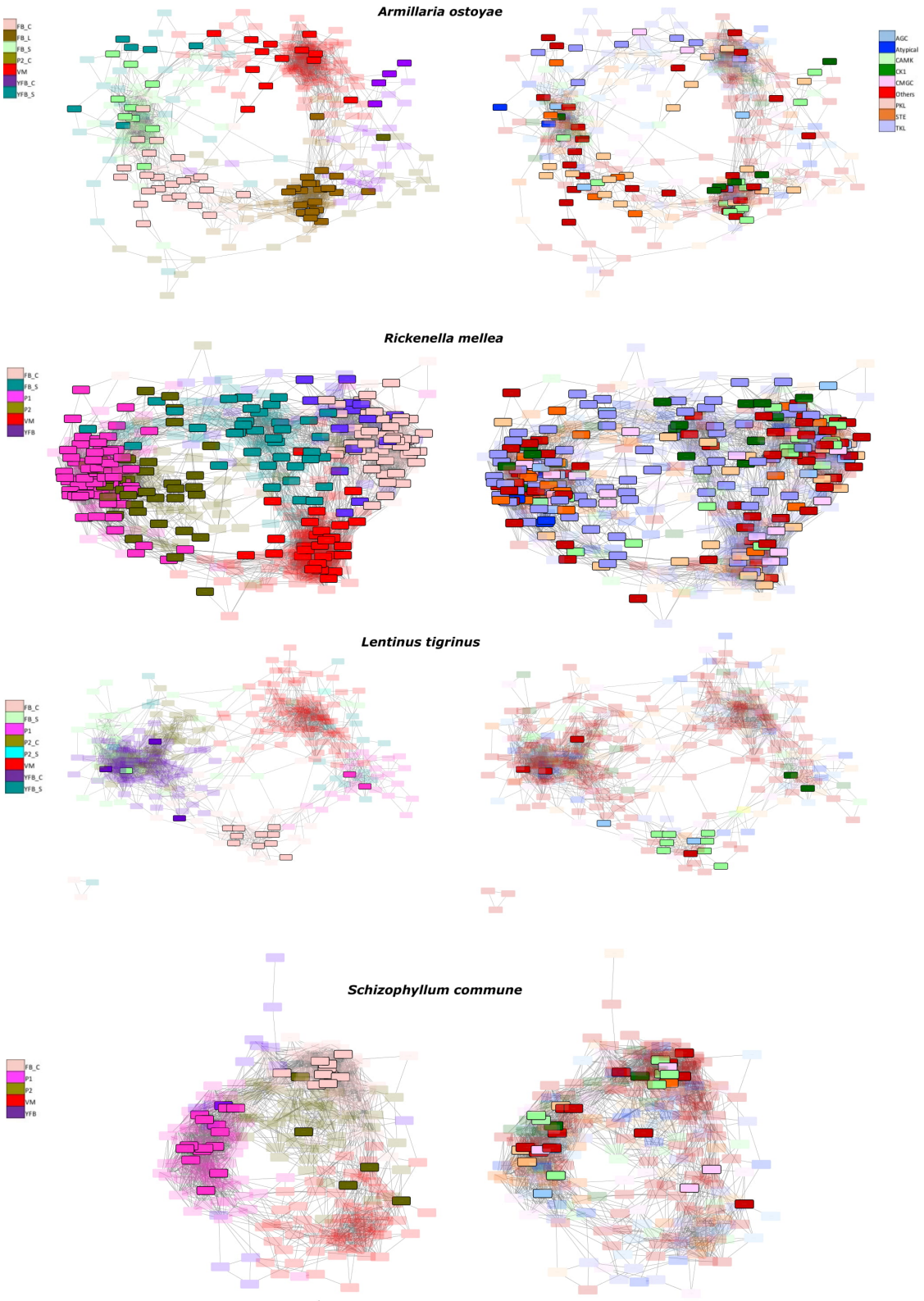

Fig S25. Kinase co-expression networks based on pairwise Pearson correlation coefficients of gene expression. Genes are colored by the gene expression maxima (left) or kinase classification (right). The developmentally regulated genes are colored, and non-developmentally regulated ones are shown by transparent rectangles.

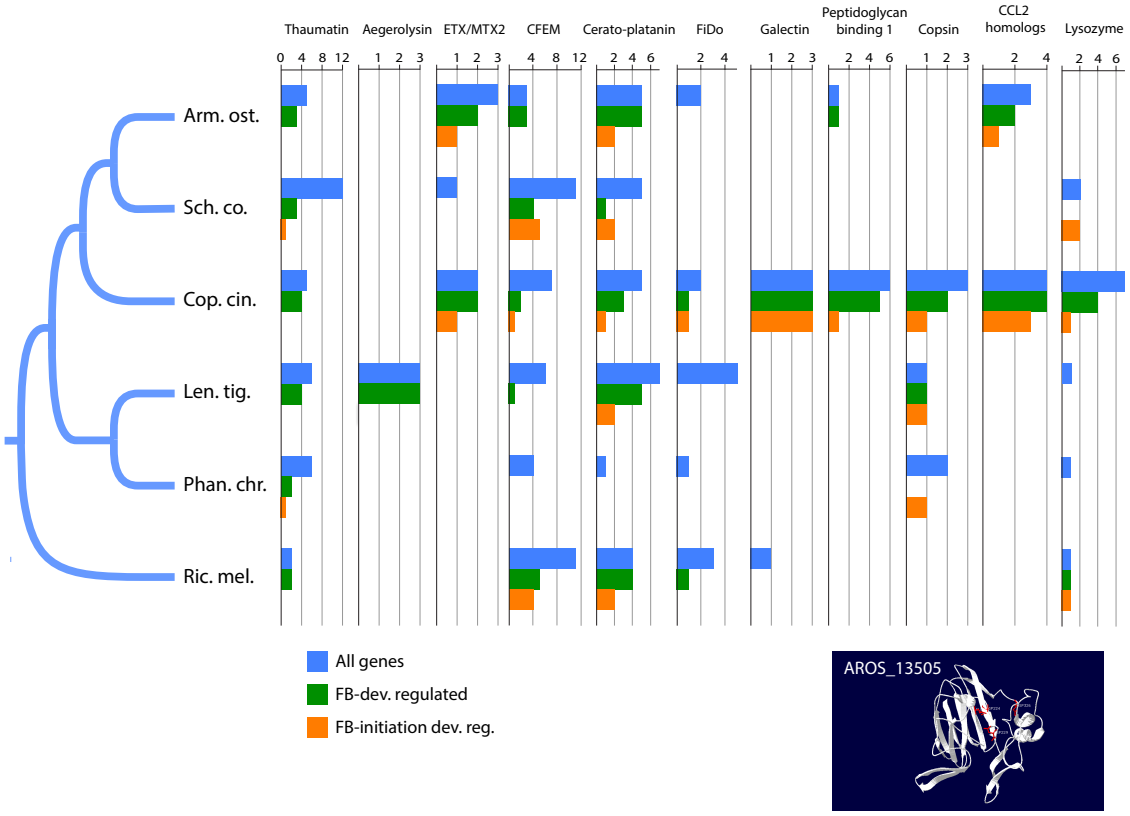

Fig. S26. Conservation and expression patterns of putative defense-related genes in six Agaricomycetes. In silico reconstructed tertiary structure of a developmentally regulated thaumatin-like protein shows an acidic cleft formed by three amino acids (red) characteristic of antimicrobial thaumatins.

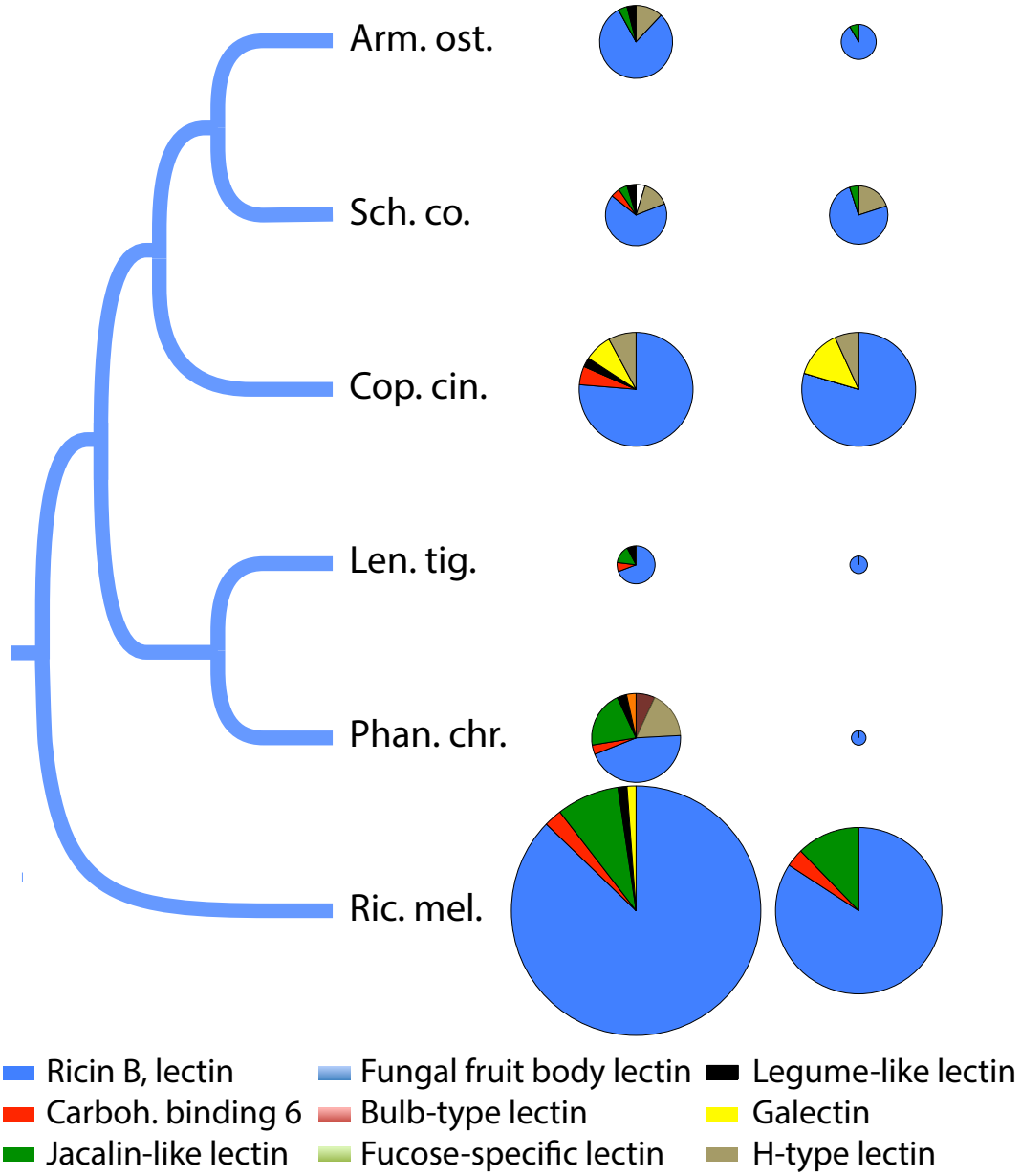

Fig. S27. Phylogenetic distribution and expression patterns of lectin-like families in six Agaricomycetes. Left panel shows the gene repertoire split by classificiation, whereas the right panel shows the composition of developmentally regulated lectin repertoires. Pie chart size proportional to the number of genes.

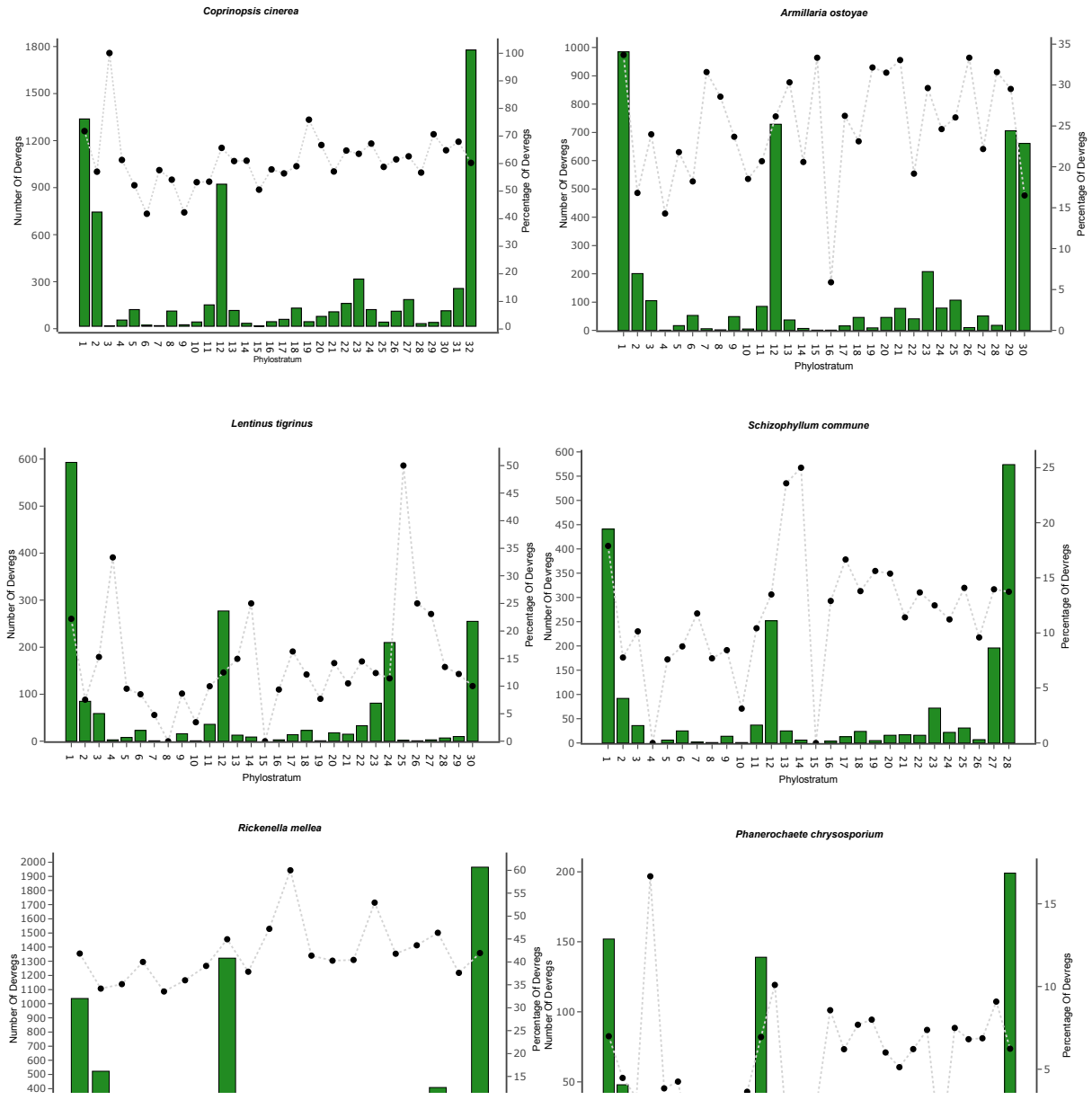

Fig. S28. Age distribution of developmentally regulated genes for five species of fruiting body forming fungi. For each species, phylostratum 1 represents the oldest gene age category (shared by all cellular organisms) while the rightmost phylostratum represents the youngest (representing species-specific genes). Green bars show the number of developmentally regulated genes per phylostratum, dashed lines show the percentage of developmentally regulated genes within each phylostratum. Phylostrata 12 and 18 represent the emergence of Dikarya and Agaricomycetes respectively (marked by asterisk).

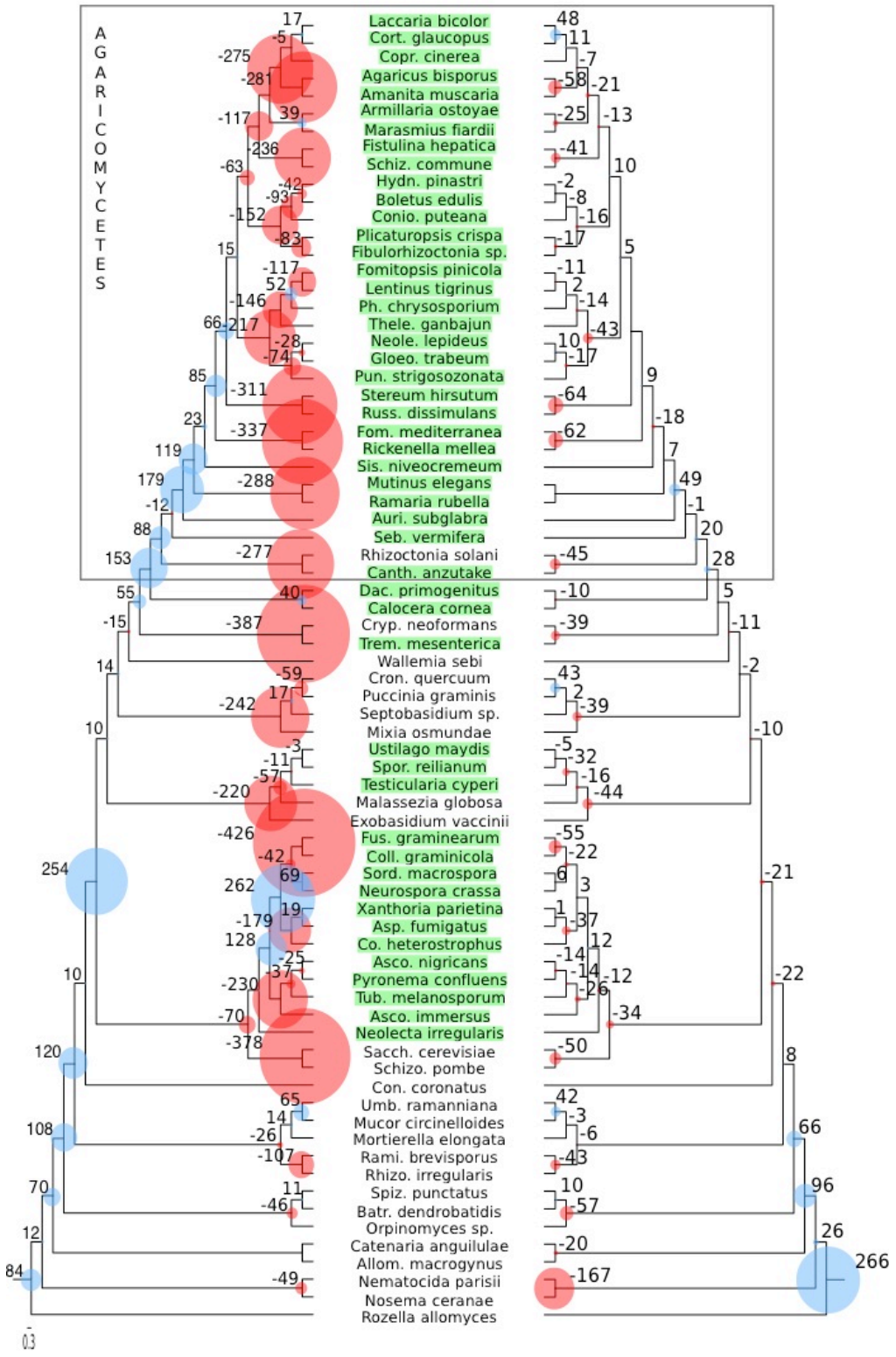

Fig. S29. Analysis of gene duplication/loss in 292 gene families containing developmentally regulated genes of 5 or 6 species (left tree) and in 290 clusters containing no or only one developmentally regulated genes (right tree). Inferred net changes to gene family size (blue circle: expansion, red

circles: contraction) are shown for all nodes (except of terminals). The species names in green are the fungi forming complex multicellular structures during the development.

Additional data table S1 (Dataset S1.xlsx)

RNA-Seq read mapping statistics for six species of Agaricomycetes.

Additional data table S2 (Dataset S2.xlsx)

Expression patterns of literature reported developmental genes of Coprinopsis. Regulation means Developmentally Regulated (DR) or not (NDR) based on our dataset.

Additional data table S3 (Dataset S3.xlsx)

IPR Enrichment analysis

Additional data table S4 (Dataset S4.xlsx)

The list and fruiting body types of 201 fungal genomes

Additional data table S5 (Dataset S5.xlsx)

Developmentally regulated genes of six Agaricomycetes.

Additional data table S6 (Dataset S6.xlsx)

Gene Ontology (GO) terms enrichment for the developmentally regulated genes of the six species.

Additional data table S7 (Dataset S7.xlsx)

Co-expression profile-wise GO enrichment.

Additional data table S8 (Dataset S8.xlsx)

Phylostratygraphy based IPR enrichment for the six species.

Additional data table S9 (Dataset S9.xlsx)

Alternative splicing events of the six species.

Additional data table S10 (Dataset S10.xlsx)

Developmentally regulated genes containing clusters.

Additional data table S11 (Dataset S11.xlsx)

Functional annotation of the developmentally regulated genes containing clusters.

Additional data table S12 (Dataset S12.xlsx)

The kinomes of the six species

References

1. Granado, J.D., Kertesz-Chaloupková, K., Aebi, M., and Kües, U. (1997). Restriction enzyme-mediated DNA integration in Coprinus cinereus. Mol. Gen. Genet. MGG *256*, 28–36.
2. Kües, U. (2000). Life history and developmental processes in the basidiomycete Coprinus cinereus. Microbiol Mol Biol Rev *64*, 316–353.
3. Ohm, R.A., De Jong, J.F., Lugones, L.G., Aerts, A., Kothe, E., Stajich, J.E., De Vries, R.P., Record, E., Levasseur, A., Baker, S.E., *et al.* (2010). Genome sequence of the model mushroom Schizophyllum commune. Nat. Biotechnol. *28*, 957–963.
4. Dons, J.J.M., De Vries, O.M.H., and Wessels, J.G.H. (1979). Characterization of the genome of the basidiomycete Schizophyllum commune. BBA Sect. Nucleic Acids Protein Synth. *563*, 100–112.
5. Hibbett, D.S., Murakami, S., and Tsuneda, A. (1993). Hymenophore Development and Evolution in Lentinus. Mycologia *85*, 428.
6. Fries, N. (1978). Basidiospore germination in some mycorrhiza-forming hymenomycetes. Trans. Br. Mycol. Soc. *70*, 319–324.
7. Sipos, G., Prasanna, A.N., Walter, M.C., O'Connor, E., Bálint, B., Krizsán, K., Kiss, B., Hess, J., Varga, T., Slot, J., *et al.* (2017). Genome expansion and lineage-specific genetic innovations in the forest pathogenic fungi Armillaria. Nat. Ecol. Evol. *1*, 1931–1941
8. Gnerre, S., MacCallum, I., Przybylski, D., Ribeiro, F.J., Burton, J.N., Walker, B.J., Sharpe, T., Hall, G., Shea, T.P., Sykes, S., *et al.* (2011). High-quality draft assemblies of mammalian genomes from massively parallel sequence data. Proc. Natl. Acad. Sci. *108*, 1513–1518.
9. Martin, J., Bruno, V.M., Fang, Z., Meng, X., Blow, M., Zhang, T., Sherlock, G., Snyder, M., and Wang, Z. (2010). Rnnotator: An automated de novo transcriptome assembly pipeline from stranded RNA-Seq reads. BMC Genomics *11*.
10. Grigoriev, I. V, Nikitin, R., Haridas, S., Kuo, A., Ohm, R., Otillar, R., Riley, R., Salamov, A., Zhao, X., Korzeniewski, F., *et al.* (2014). MycoCosm portal: Gearing up for 1000 fungal genomes. Nucleic Acids Res. *42*.
11. Robinson, M.D., McCarthy, D.J., and Smyth, G.K. (2010). edgeR: a Bioconductor package for differential expression analysis of digital gene expression data. Bioinformatics *26*, 139–140.
12. Robinson, M.D., and Oshlack, A. (2010). A scaling normalization method for differential expression analysis of RNA-seq data. Genome Biol. *11*.
13. Ritchie, M.E., Phipson, B., Wu, D., Hu, Y., Law, C.W., Shi, W., and Smyth, G.K. (2015). Limma powers differential expression analyses for RNA-sequencing and microarray studies. Nucleic Acids Res. *43*, e47.
14. Enright, A.J., Van Dongen, S., and Ouzounis, C.A. (2002). An efficient algorithm for large-scale detection of protein families. Nucleic Acids Res. *30*, 1575–1584.
15. Gehrmann, T., Pelkmans, J.F., Lugones, L.G., Wösten, H.A.B., Abeel, T., and Reinders, M.J.T. (2016). Schizophyllum commune has an extensive and functional alternative splicing repertoire. Sci. Rep. *6*.
16. Dobin, A., Davis, C.A., Schlesinger, F., Drenkow, J., Zaleski, C., Jha, S., Batut, P., Chaisson, M., and Gingeras, T.R. (2013). STAR: Ultrafast universal RNA-seq aligner. Bioinformatics *29*, 15–21.
17. Trapnell, C., Williams, B.A., Pertea, G., Mortazavi, A., Kwan, G., Van Baren, M.J., Salzberg, S.L., Wold, B.J., and Pachter, L. (2010). Transcript assembly and quantification by RNA-Seq reveals unannotated transcripts and isoform switching during cell differentiation. Nat. Biotechnol. *28*, 511–515.
18. Mancini, E., Iserte, J., Yanocsky, M., and Chernomoretz, A. (2017). ASpli: An integrative R package for analysing alternative splicing using RNAseq - Semantic Scholar.

19. Domazet-Lošo, T., Brajković, J., and Tautz, D. (2007). A phylostratigraphy approach to uncover the genomic history of major adaptations in metazoan lineages. Trends Genet. *23*, 533–539.
20. Drost, H.G., Gabel, A., Grosse, I., and Quint, M. (2015). Evidence for active maintenance of phylotranscriptomic hourglass patterns in animal and plant embryogenesis. Mol. Biol. Evol. *32*, 1221–1231.
21. Torruella, G., De Mendoza, A., Grau-Bové, X., Antó, M., Chaplin, M.A., Del Campo, J., Eme, L., Pérez-Cordón, G., Whipps, C.M., Nichols, K.M., *et al.* (2015). Phylogenomics Reveals Convergent Evolution of Lifestyles in Close Relatives of Animals and Fungi. Curr. Biol. *25*, 2404–2410.
22. Darling, A.E., Carey, L., and Feng, W.-C. (2003). The Design, Implementation, and Evaluation of mpiBLAST. In ClusterWorld Conference & Expo and the 4th International Conference on Linux Clusters: The HPC Revolution.
23. Nagy, L.G., Ohm, R.A., Kovács, G.M., Floudas, D., Riley, R., Gácser, A., Sipiczki, M., Davis, J.M., Doty, S.L., de Hoog, G.S., *et al.* (2014). Latent homology and convergent regulatory evolution underlies the repeated emergence of yeasts. Nat. Commun. *5*, 4471.
24. Katoh, K., Misawa, K., Kuma, K., and Miyata, T. (2002). MAFFT: a novel method for rapid multiple sequence alignment based on fast Fourier transform. Nucleic Acids Res. *30*, 3059–66.
25. Stamatakis, A. (2015). Using RAxML to Infer Phylogenies. Curr. Protoc. Bioinforma. *51*, 6.14.1-14.
26. Capella-Gutierrez, S., Silla-Martinez, J.M., and Gabaldon, T. (2009). trimAl: a tool for automated alignment trimming in large-scale phylogenetic analyses. Bioinformatics *25*, 1972–1973.
27. Durand, D., Halldórsson, B. V., and Vernot, B. (2006). A Hybrid Micro–Macroevolutionary Approach to Gene Tree Reconstruction. J. Comput. Biol. *13*, 320–335.
28. Nagy, L.G., Riley, R., Bergmann, P.J., Krizsán, K., Martin, F.M., Grigoriev, I. V., Cullen, D., and Hibbett, D.S. (2017). Genetic Bases of Fungal White Rot Wood Decay Predicted by Phylogenomic Analysis of Correlated Gene-Phenotype Evolution. Mol. Biol. Evol. *34*, 35–44.
29. Lombard, V., Golaconda Ramulu, H., Drula, E., Coutinho, P.M., and Henrissat, B. (2014). The carbohydrate-active enzymes database (CAZy) in 2013. Nucleic Acids Res. *42*.
30. Levasseur, A., Drula, E., Lombard, V., Coutinho, P.M., and Henrissat, B. (2013). Expansion of the enzymatic repertoire of the CAZy database to integrate auxiliary redox enzymes. Biotechnol. Biofuels *6*.
31. Ernst, J., and Bar-Joseph, Z. (2006). STEM: A tool for the analysis of short time series gene expression data. BMC Bioinformatics *7*.
32. Ernst, J., Nau, G.J., and Bar-Joseph, Z. (2005). Clustering short time series gene expression data. Bioinformatics *21*.
33. Pierleoni, A., Martelli, P., and Casadio, R. (2008). PredGPI: a GPI-anchor predictor. BMC Bioinformatics *9*, 392. Available at:
34. Petersen, T.N., Brunak, S., Von Heijne, G., and Nielsen, H. (2011). SignalP 4.0: Discriminating signal peptides from transmembrane regions. Nat. Methods *8*, 785–786.
35. Pellegrin, C., Morin, E., Martin, F.M., and Veneault-Fourrey, C. (2015). Comparative Analysis of Secretomes from Ectomycorrhizal Fungi with an Emphasis on Small-Secreted Proteins. Front. Microbiol. *6*, 1278.
36. Horton, P., Park, K.J., Obayashi, T., Fujita, N., Harada, H., Adams-Collier, C.J., and Nakai, K. (2007). WoLF PSORT: Protein localization predictor. Nucleic Acids Res. *35*.

37. Melén, K., Krogh, A., and Von Heijne, G. (2003). Reliability measures for membrane protein topology prediction algorithms. J. Mol. Biol. *327*, 735–744.
38. Shelest, E. (2017). Transcription Factors in Fungi: TFome Dynamics, Three Major Families, and Dual-Specificity TFs. Front. Genet. *8*, 53.
39. Chen, L., Gong, Y., Cai, Y., Liu, W., Zhou, Y., Xiao, Y., Xu, Z., Liu, Y., Lei, X., Wang, G., *et al.* (2016). Genome Sequence of the Edible Cultivated Mushroom Lentinula edodes (Shiitake) Reveals Insights into Lignocellulose Degradation. PLoS One *11*, e0160336.
40. Stajich, J.E., Wilke, S.K., Ahren, D., Au, C.H., Birren, B.W., Borodovsky, M., Burns, C., Canback, B., Casselton, L.A., Cheng, C.K., *et al.* (2010). Insights into evolution of multicellular fungi from the assembled chromosomes of the mushroom Coprinopsis cinerea (Coprinus cinereus). Proc Natl Acad Sci U S A *107*, 11889–11894.
41. Manning, G., Whyte, D.B., Martinez, R., Hunter, T., and Sudarsanam, S. (2002). The protein kinase complement of the human genome. Science (80-.). *298*, 1912–1934.
42. Muraguchi, H., and Kamada, T.A. (2000) A mutation in the *eln2* gene encoding a cytochrome P450 of Coprinus cinereus affects mushroom morphogenesis. Fungal Genet Biol *29***,** 49-59.
43. Cheng, C.K., Au, C.H., Wilke, S.K., Stajich, J.E., Zolan, M.E., Pukkila, P.J., and Kwan, H.S. (2013) 5'-Serial Analysis of Gene Expression studies reveal a transcriptomic switch during fruiting body development in Coprinopsis cinerea. PloS One *10*, 1-17.
44. Yoon, J.-J., Munir, E., Miyasou, H., Hattori, T., Shimada, M., and Terashita, T. (2002) A possible role of the key enzymes of the glyoxylate and gluconeogenesis pathways for fruit-body formation of the wood-rotting basidiomycete Flammulina velutipes. Mycoscience *43*, 327-332.
45. Moore, D., Elhiti, M.M.Y., Butler, R.D. (1979) Morphogenesis of the carpophore of *Coprinopsis cinereus*. New Phytol *83*, 695-722.
46. Feng, K., Wang, L.Y., Liao, D.-J., Lu, X.-P., Hu, D.-J., Liang, X., Zhao, J., Mo, Z.-Y., and Li, S.-P. (2017) Potential molecular mechanisms for fruiting body formation of Cordyceps illustrated in the case of Cordyceps sinensis. Mycology *8*, 231-258.
47. Burton, K.S., Partis, M-D., Wood, D.A., and Thurston, C.F. (1997) Accumulation of serine proteinase in senescent sporophores of the cultivated mushroom, *Agaricus bisporus.* Mycol Res *101*, 146-152.
48. Elleuche, S. and Pöggeler, S. (2010) Carbonic anhydrases in fungi. Microbiology *156*, 23-29.
49. Hock, B., Bahn, M., Walk, R. A., Nitschke, U. (1978) The control of fruiting body formation in the ascomycete Sordaria macrospora Auersw. by regulation of hyphal development : An analysis based on scanning electron and light microscopic observations. Planta *141*, 93-103.
50. Ferguson, S.M. and De Camilli, P. (2012) Dynamin, a membrane remodelling GTPase. Nat Rev Mol Cell Biol *13*, 75-88.
51. Kühlbrandt, W. (2004) Biology, structure and mechanism of P-type ATPases. *Nat* Rev Mol Cell Biol *5*, 282-295.
52. Gilman, B., Tijerine, P., Russel, R. (2017) Distinct RNA-unwinding mechanisms of DEAD-box and DEAH-box RNA helicase proteins in remodeling structured RNAs and RNPs. Biochem Soc Trans *45*, 1313-1321.
53. Miller, M.T., Higgin, J.J., Hall, T.M. (2008) Basis of altered RNA-binding specificity by PUF proteins revealed by crystal structures of yeast Puf4p. Nat Struct Mol Biol *15*, 397-402.
54. Wessels, J.G.H. (1996) Fungal hydrophobins: proteins that function at an interface. Trends Plant Sci *1*, 9-15.
55. Nehls, U. and Dietz, S. (2014) Fungal aquaporins: cellular functions and ecophysiological perspectives. Appl Microbiol Biotechnol *98*, 8835-8851.

56. Künzler, M. (2015) Hitting the sweet spot-glycans as target of fungal defense effector proteins. Molecules *20*, 8144-8167.
57. Sakamoto, Y., Watanabe, H., Nagai, M., Nakade, K., Takahashi, M., Sato, T. (2006) *Lentinula edodes tlg1* encodes thaumatin-like protein that is involved in lentinan degradation and fruiting body senescence. Plant Physiol *141*, 793-801.
58. Tao, Y., van Peer, A.F., Chen, B., Chen, Z., Zhu, J., Deng, Y., Jiang, Y., Li, S., Wu, T., Xie, B. (2014) Gene expression profiling reveals large regulatory switches between succeding stipe stages in *Volvariella volvacea.* PloS One *9*, 1-10.
59. Muraguchi H, et al. (2015) Strand-specific RNA-seq analyses of fruiting body development in Coprinopsis cinerea. *PLoS One* 10(10). doi:10.1371/journal.pone.0141586.